STUDIES OF THE EFFECTS OF ELECTROLYTE ADDITIVES ON THE REACTIVITY BETWEEN CHARGED ELECTRODES AND ELECTROLYTES IN LI-ION BATTERIES USING ACCELERATING RATE CALORIMETRY

by

Lin Ma

Submitted in partial fulfilment of the requirements
for the degree of Master of Science
at

Dalhousie University
Halifax, Nova Scotia
July 2014

To my parents and my friends

TABLE OF CONTENTS

LIST OF TABLES

LIST OF FIGURES

ABSTRACT

Electrolyte additives can extend lifetime of Li-ion cells because they can modify the solid electrolyte interphase (SEI) on the negative electrode and the passivation layer on the positive electrode. Electrolyte additives affect the reactions between the charged electrodes and electrolytes at high temperature and may impact the safety of Li-ion cells. In order to be able to distinguish the effects of an additive or additive blends on the reactivity of positive or negative electrodes with electrolytes at elevated temperatures, an experimental method has been developed based on accelerating rate calorimetry (ARC). This method proved to be useful and showed that selected additives affected the reaction between lithiated graphite and electrolytes more than that between delithiated $Li(Ni_{1/3}Mn_{1/3}Co_{1/3})O_2$ and electrolytes. Some of the selected additives or additive combinations dramatically decreased the self-heating rate compared to control electrolyte. Incorporating such additives or additive combinations into Li-ion cells should lead to safer Li-ion cells.

LIST OF ABBREVIATIONS USED

α	Fractional Degree of Conversion of Reactants
A	Pre-exponential Factor
ARC	Accelerating Rate Calorimetry
BET	Brunauer-Emmett-Teller
CE	Coulombic Efficiency
C_{tot}	Total Heat Capacity
DEC	Diethyl Carbonate
DMC	Dimethyl Carbonate
DTD	Ethylene Sulfate
E_a	Activation Energy
EC	Ethylene Carbonate
EMC	Ethyl Methyl Carbonate
EMS	Ethyl Methyl Sulfone
FEC	Fluoro Ethylene Carbonate
GC-MS	Gas Chromatography-Mass Spectroscopy
h	Total Heat
IRC	Irreversible Capacity Loss
LCO	$LiCoO_2$
LiBOB	$LiB(C_2O_4)_2$
LEDC	$(CH_2OCO_2Li)_2$
$LiMO_2$	Lithium Transition Metal Dioxide
LiFSI	$LiN(SO_2F)_2$
LiTFSI	$LiN(SO_2CF_3)_2$
LTO	$Li_4Ti_5O_{12}$
MMDS	Methylene Methanedisulfonate
NMC	$Li(Ni_{1/3}Mn_{1/3}Co_{1/3})O_2$
NMP	N-methyl Pyrrolidone
PC	Propylene Carbonate
PES	Prop-1-ene-1,3-Sultone
PLS	Propylene Sulfate
PVDF	Polyvinylidene Fluoride
R	Universal Gas Constant
SHR	Self-heating Rate
SEI	Solid Electrolyte Interphase
SEM	Scanning Electron Microscopy
T	Kelvin Temperature
TMS	1,3- Propylene Sulfate
TTSP	Tris(trimethylsilyl) Phosphate
TTSPi	Tris(trimethylsilyl) Phosphite
VC	Vinylene Carbonate
VEC	Vinyl Ethylene Carbonate

ACKNOWLEDGEMENTS

First I would like to thank NSERC and 3M, for financial support.

I would like to give special thanks to my supervisor Dr. Jeff Dahn for providing the best research atmosphere and equipment in our lab. Without his help, I could not finish this work. I would also like to thank my committee members, Dr. Peng Zhang and Dr. Mark Obrovac for their invaluable help and advice. I am also very grateful for the administrative help from Giselle Andrews.

Most importantly I would like to give thanks to the Chinese group in the Dahn lab (Xin Xia, Deijun Xiong, Jian Xia, Ping Ping, Sirong Li, Zhiyong Yu, Mengyun Nie, Xiaowei Ma, Jing Li, David Wang and so on). It is not easy for Chinese people to get together in Canada and work on the same team. I am infinitely grateful for the help from Chinese group in this lab.

I would like to thank all Dahn lab members. Thanks to Dave for helping me install software, setting up the new ARC and arranging UHPC channels. Thanks to Robbie for fixing the machines we use every day and teaching me about all kinds of machines. Thanks to Simon for cutting ARC tubes and fixing the new ARC top lid. Thanks to John for teaching me all kinds of stuff such as how to BBQ, how to apply for travel reimbursement, how to do XRD perfectly and so on. Thanks to Rémi, Chris Burns, Laura, Reza and Chris Kim for very useful discussion about research. Thanks to Lenaic for teaching me how to use XPS. Thanks to Kathlyne for organizing social events. Thanks to Ramesh and Tim for useful talks about life. Thanks to Aaron, Patrick, Connor, Steven, Colby, Julian and others who have left the group such as Eric, Jennifer and Nupur. Thanks to all the summer students.

Finally I would give thousands of thanks to my parents for endless spiritual encouragement and support.

CHAPTER 1. INTRODUCTION

1.1 MOTIVATION

Lithium-ion batteries are used in portable electronics (laptops, mobile phones, cameras, etc.) and in electrified vehicles. In 2013, five billion lithium-ion cells were produced for consumer electronics.[1] However, the cost of lithium-ion batteries may limit their use in electrified vehicles.

There are many ways of decreasing the cost of lithium-ion batteries,[2] such as using lower cost materials, increasing packaging efficiency, increasing manufacturing yields and so on. Extending the lifetime of lithium-ion cells is also an important method of decreasing the replacement cost from a practical and financial point of view.

Parasitic reactions between the charged positive or negative electrodes and the electrolyte are one reason for the finite lifetime of lithium-ion cells because these can deplete the supply of active lithium or electrolyte. The use of electrolyte additives can improve cell lifetime by modifying the properties of the SEI and thus lead to a decrease in the rate of parasitic reactions.[3,4] Xiong et al.[5] and Burns et al.[6] showed that vinylene carbonate (VC), a famous and widely used additive, affected both the positive and negative electrodes by reducing the charge endpoint capacity slippage and improving the coulombic efficiency (CE). Xia et al.[7,8] showed that some sulfur-containing electrolyte additives could help extend the lifetime of lithium-ion cells by increasing the coulombic efficiency (CE) and decreasing impedance when used alone or when combined with VC. Xu et al.[9] showed that the capacity retention of $Li/LiNi_{0.5}Mn_{1.5}O_4$ cells improved with the

addition of dimethyl methylphosphonate (DMMP). X-ray Photoelectron Spectroscopy (XPS) and Infrared (IR) spectroscopy suggested that the addition of DMMP could inhibit electrolyte decomposition on the surface of the positive electrode.

Although electrolyte additives can make a contribution to improving electrochemical performance, they may also affect the safety of Li-ion cells.[10] Therefore, the effect of electrolyte additives on electrode/electrolyte reactivity at elevated temperatures (> 100°C) must be carefully studied.

For university researchers, ARC is a suitable method for fundamental studies of the reactions between charged electrode materials and electrolyte at elevated temperatures. In 1998, Richard and Dahn[11,12] designed a method to study the thermal stability of lithiated graphite in 1M $LiPF_6$/EC:DEC (different ratios) electrolyte using ARC. MacNeil and Dahn[13] studied the impact of surface area on the reactivity of various lithiated carbon negative electrode materials with electrolyte. Zhou et al.[14] studied the impact of Al substitution for Co on the reactivity of charged $Li(Ni_{1/3}Mn_{1/3}Co_{1/3})O_2$ (NMC111) with electrolyte. They found that Al substitution caused a dramatic decrease of the reactivity. Xia et al.[15] studied the effect of triphenylphosphate (TPP), a flame retardant additive, on the reactivity between lithiated graphite or delithiated NMC with non-aqueous electrolytes using ARC. They found that the addition of TPP did not increase the reactivity of the lithiated graphite electrode but did increase the reactivity of charged NMC. Gnanaraj et al.[16] compared the thermal stability of several salts ($LiPF_6$, $LiClO_4$, $LiN(SO_2CF_2CF_3)_2$ and $LiPF_3(CF_2CF_3)_3$) in electrolyte solutions (mixtures of ethylene carbonate, dimethyl carbonate and diethyl carbonate) using ARC.

$LiN(SO_2CF_2CF_3)_2$-containing electrolyte was found to be the most thermally stable solution while $LiClO_4$-containing solutions had the lowest thermal stability.

This thesis presents a series of comparative studies of the effects of some promising electrolyte additives or combinations of additives on the reactivity of charged positive or negative electrode materials of Li-ion cells with non-aqueous electrolytes. The next section of this chapter will present an introduction to lithium-ion cells and common electrode materials. A brief review of the surface chemistry of the electrode/electrolyte interphases is also given. Chapter 2 describes the experimental techniques and relevant theory used throughout this project. A discussion and interpretation of experimental methods used for this thesis will be presented in Chapter 3. Chapter 4 gives results obtained about the reactivity of lithiated graphite or delithiated NMC in non-aqueous electrolytes containing selected additives or additive combinations.

1.2 BASIC CONFIGURATION AND ELECTROCHEMISTRY FOR LI-ION BATTERIES

Generally, lithium-ion batteries are comprised of electrodes materials (lithium intercalation compounds) and lithium salt-containing electrolyte.[17] Figure 1.1 shows a schematic of a lithium-ion cell with a $Li(Ni_{1/3}Mn_{1/3}Co_{1/3})O_2$ (NMC111) positive electrode and a graphite negative electrode. NMC and graphite are the main materials used in this thesis. The positive electrode material is typically a lithium transition metal oxide with a layered structure. The material is attached to an aluminum foil current

collector. The negative electrode is typically graphite particles attached to a copper current collector. The two electrodes are separated by a separator (typically made of porous polyolefin) which allows ion flow but prevents electric contact between the electrodes.[18]

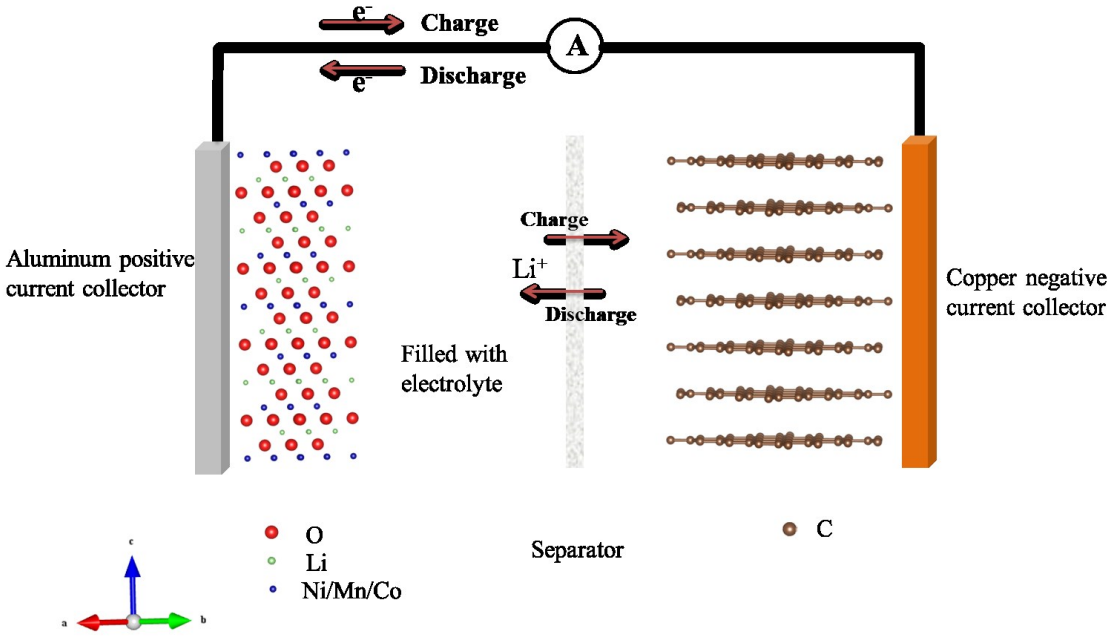

Figure 1.1 Schematic of a lithium-ion cell with a $Li(Ni_{1/3}Mn_{1/3}Co_{1/3})O_2$ (NMC) positive electrode (left) and a graphite negative electrode (right).

During the charge/discharge process, lithium ions are reversibly inserted between or extracted from atomic layers of the active materials without damaging their structures. When lithium-ion cells are charged, the electrons are forced to move from the positive electrode to the negative electrode through an external circuit and the corresponding lithium-ions de-intercalate from the positive electrode then travel through the electrolyte to insert in the negative electrode. During the discharge process, the directions of

electron and ion flows are opposite to that of the charging process. The reactions below describe the charge/discharge reaction at the positive and negative electrode, respectively, where M represents a transition metal or combinations of transition metals. During charge the forward reaction occurs while the reverse reaction occurs during discharge.

$$LiMO_2 \leftrightarrow Li_{1-y}MO_2 + yLi^+ + ye^- \quad (1.1)$$

$$C_6 + xLi^+ + xe^- \leftrightarrow Li_xC_6 \quad (1.2)$$

Figure 1.2 shows the voltage versus specific capacity of $Li(Ni_{1/3}Mn_{1/3}Co_{1/3})O_2$/Li (a) and graphite/Li (b) coin cells charged and discharged at C/10 and at a temperature of 30°C for many cycles, respectively. In panel (a), the initial capacity does not return to zero on the x axis, which is due to a difference between the initial charge and discharge capacity called the first cycle irreversible capacity loss (IRC).[19] Furthermore, a continued shift to the right, referred to as charge endpoint capacity slippage, continues with cycling as shown in Figure 1.2(a). The initial IRC is generally much larger than the subsequent slippage during every cycle. Charge endpoint capacity slippage[20,21] gives an indication of the amount of parasitic reactions occurring at the positive electrode, such as oxidation of electrolyte.

A similar analysis can be used for graphite/Li half cells. Figure 1.2(b) shows the first cycle irreversible capacity loss (IRC) caused by the reaction of the electrolyte with lithium at the surface of the negative electrode to form the so-called SEI.[22] The slippage of the voltage curve also continues with cycling as the SEI thickens.[23] Some details about the SEI will be discussed in the next section of this chapter.

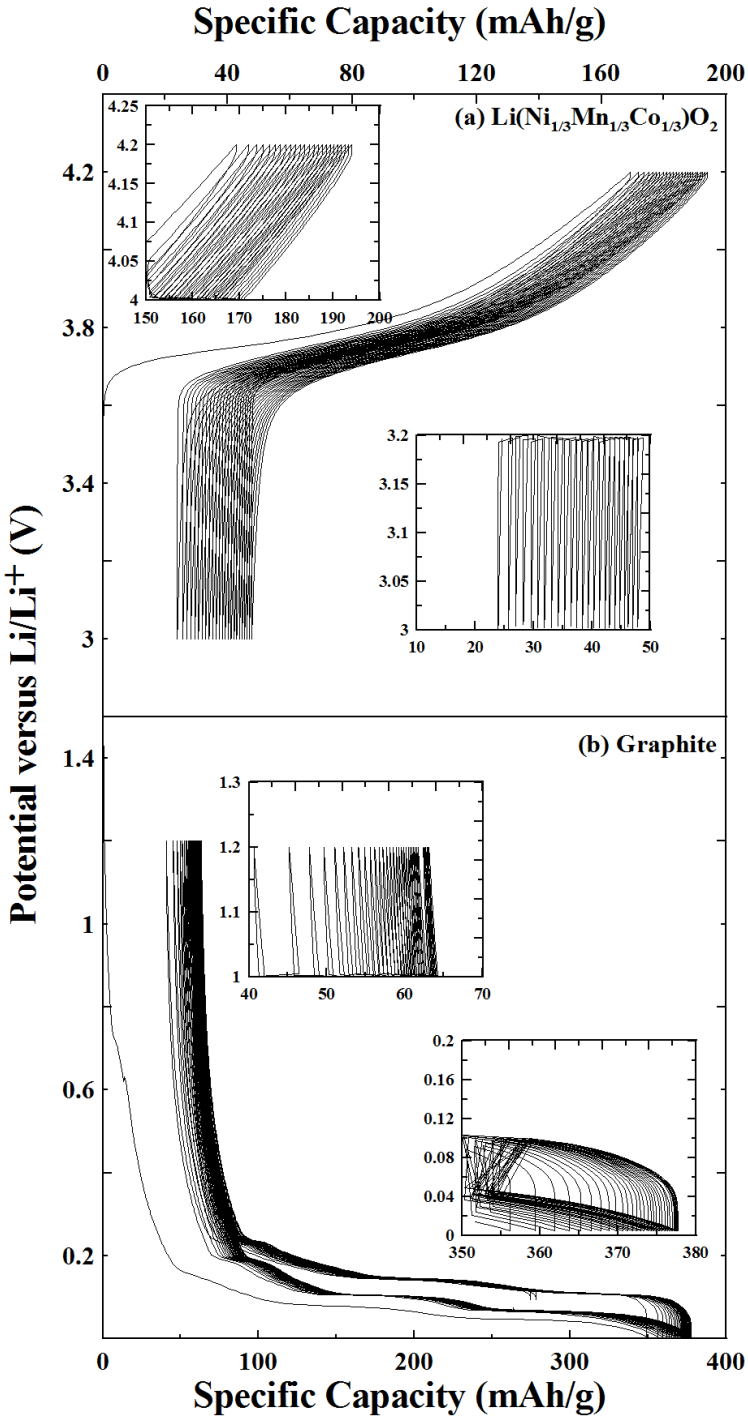

Figure 1.2 Potential versus specific capacity for (a) NMC/Li half cell over 24 cycles between 3.0 and 4.2 V, (b) a graphite/Li half cell over 34 cycles between 0.005 and 1.2 V at 30°C. The current corresponds to a C/10 rate.

1.3 ELECTRODES IN LI-ION BATTERIES

Electrode materials with high energy density, high power, better safety performance, lower toxicity and lower cost are desired for applications such as electric vehicles (EV).[24,25] The most commonly used positive electrode materials can be broadly classified into the following three types based on their crystallographic structures:

- Layered materials (e.g. $Li[M]O_2$, M = Co, Ni, Mn, etc.)
- Spinel materials (e.g. $LiMn_2O_4$)
- Olivine materials (e.g. $Li[M]PO_4$, M = Fe, Co, Mn, etc.)

Since the current research related to the positive electrode has been exclusively performed on $Li(Ni_{1/3}Mn_{1/3}Co_{1/3})O_2$ which is a layered material, only a detailed discussion about layered materials will be presented in this thesis.

The general formula $Li[M]O_2$ can be used to represent layered lithium transition metal oxides, where M represents a single 3d transition metal[26] or a combination of 3d transition metals.[14,27] In this general formula, $Li(Ni_{1/3}Mn_{1/3}Co_{1/3})O_2$ (NMC111) is a popular replacement for $LiCoO_2$ (LCO) because cobalt is expensive and the reactivity of charged NMC111 with electrolyte is less severe than that of charged LCO.[28] In NMC111, Mn remains at an oxidation state of +4 during the charge and discharge process while Ni and Co provide the electrochemical activity.[29,30] The Ni^{2+}/Ni^{4+} couple is responsible for most of the cycling capacity. Ohzuku et al.[31] showed that NMC111 could deliver a reversible capacity of ~ 150 mAh/g between 3.5 - 4.2 V. Based on lower cost,

comparable capacity and, in particular, better safety performance, NMC111 has become an attractive and commercialized positive material.

Currently graphite is used as the negative electrode material for most lithium-ion batteries because of its low operating potential versus Li/Li^+, improved safety compared to metallic lithium and relatively high specific capacity. Graphite is comprised of parallel sheets containing interconnected hexagons of carbon, namely graphene sheets.[32] These sheets are stacked with ABAB stacking in the notation of close packed planes. This stacking sequence changes from ABAB… to AA… when lithium is intercalated into the graphite. The process of lithium intercalation and de-intercalation can be repeated thousands of times without destroying the structure of graphite. The specific capacity of graphite can reach 372 mAh/g if the maximum concentration of one Li per six carbons, LiC_6, is reached.

Several other negative electrode materials such as $Li_4Ti_5O_{12}$ (LTO), silicon and tin, etc. have received attention but they are not commonly used. LTO has specific capacity of 175 mAh/g and its operating voltage is 1.5 V versus Li/Li^+,[33] which results in lower energy density. Alloy materials such as Sn[34,35] or Si[36,37] have higher specific capacities compared to graphite but these capacities are accompanied by a large volume expansion upon lithiation, which causes poor capacity retention over many cycles.

1.4 ELECTROLYTES AND INTERPHASES

In addition to the positive and negative electrodes, the electrolyte is another significant and complex part of lithium-ion batteries. The main components of lithium-ion battery

electrolytes are solvents, lithium salts and additives and they will be discussed, respectively, in the next section. Furthermore, some electrolyte components are typically sacrificed to form a protective film on the surface of the electrodes to avoid sustained reduction or oxidation of the electrolytes during cycling. The protective films are named SEI, which strongly impact battery performance and have been the focus of lithium-ion battery research.

1.4.1 ELECTROLYTE SYSTEM

1.4.1.1 Solvents

Ethylene carbonate (EC) is the most common electrolyte solvent because of its high dielectric constant, which permits good ionic dissociation of the salt, good compatibility with the commonly used electrode materials, good film forming properties and so on.[38] In order to expand the limited liquid range of EC-based electrolytes, linear carbonates (e.g. dimethyl carbonate (DMC), ethyl methyl carbonate (EMC) or diethyl carbonate (DEC)) are mixed with EC. EC:DEC (1:2 by volume) and EC:EMC (3:7 by mass) are commonly used solvent mixtures. These solvent mixtures are compatible with common electrode materials and have wide enough stable electrochemical windows. The structures of the molecules mentioned above are shown in Figure 1.3.

Efforts are being made to replace carbonate-based electrolyte solvents to enable high voltage lithium-ion batteries.[39] Sulfones[40] and nitriles[41] are promising candidates because of their resistance against oxidation. Ethyl methyl sulfone (EMS) and tetramethylene

sulfone (TMS) (see Figure 1.3) were tested in $Li_4Ti_5O_{12}/LiNi_{0.5}Mn_{1.5}O_4$ cells and showed good capacity retention.[40]

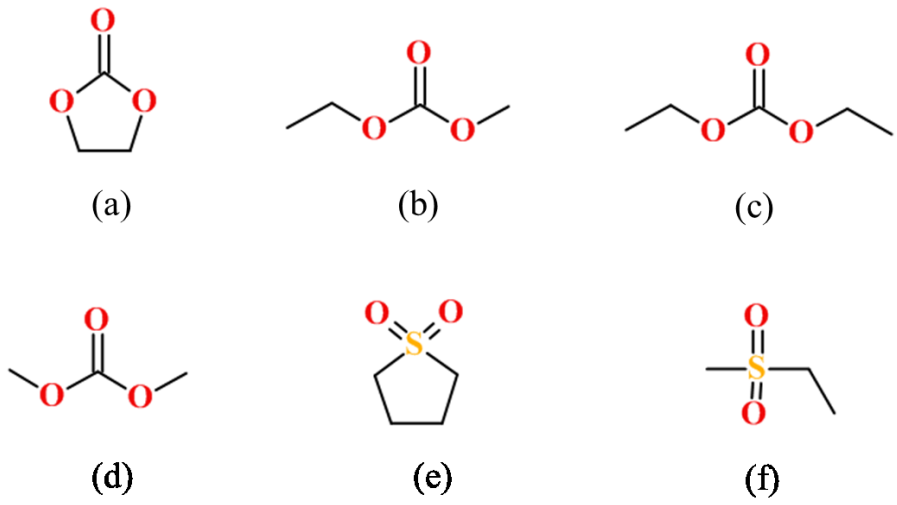

Figure 1.3 Chemical structures of some solvents used in lithium-ion batteries: (a) ethylene carbonate (EC), (b) ethyl methyl carbonate (EMC), (c) diethyl carbonate (DEC), (d) dimethyl carbonate (DMC), (e) tetramethylene sulfone (TMS) and (f) ethyl methyl sulfone (EMS).

1.4.1.2 Salts

Lithium hexafluorophosphate, $LiPF_6$, is used in most Li-ion batteries because of its well-balanced properties[17] such as high ionic conductivity (> 10^{-3} S/cm), high lithium ion transference number (~ 0.35), passivation of the Al positive electrode current collector[42] and so on. However, its chemical and thermal instability[43] result in some potential issues. Other commonly used salts are lithium tetrafluoroborate ($LiBF_4$),[44] lithium bis(oxalato)borate (LiBOB),[45] lithium bis (trifluoromethanesulfonyl)imide

((LiN(SO_2CF_3)$_2$ called LiTFSI)[46] and lithium bis(fluorosulfonyl)imide ($LiNS_2O_4F_2$ called LiFSI).[47] Figure 1.4 shows the schematic structures of the salts mentioned above.

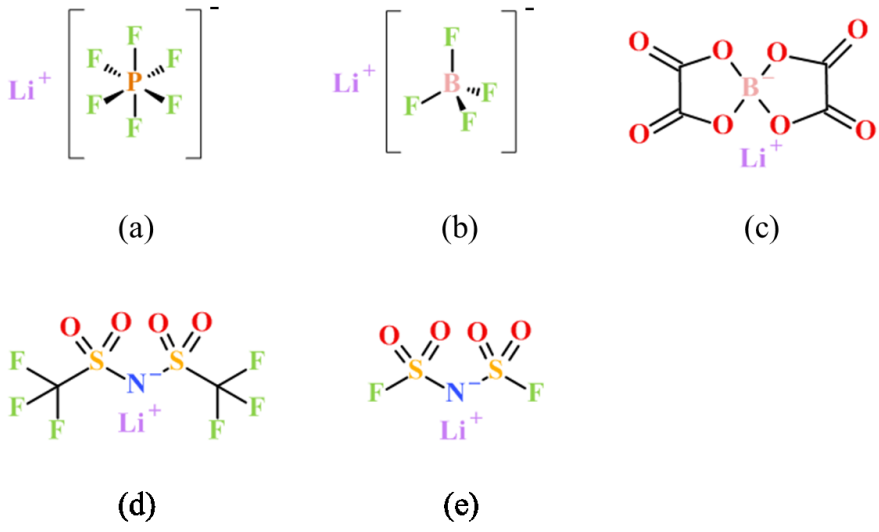

Figure 1.4 Schematic structures of some common salts used in lithium-ion batteries: (a) $LiPF_6$ (b) $LiBF_4$ (c) LiBOB (d) LiTFSI and (e) LiFSI.

1.4.1.3 Additives

The use of electrolyte additives (chemicals added at the 0.1-10% level[38]) is an efficient and economical way to improve cell performance without entirely replacing the major components of the electrolyte. Several years ago, Zhang et al.[48] and Xu et al.[38] wrote extensive reviews about different electrolyte additives. Based on their reports, the function of electrolyte additives can be generally divided into the following two categories: (1) modifying the properties of the SEI on the negative electrode or the

passivation layer on the positive electrode; (2) and protecting cells from overcharging. This thesis will focus on additives that modify the SEI and passivation layers, which have an impact on cell calendar life, impedance and safety. The effect of electrolyte additives on the SEI and passivation layers will be discussed in the next section.

Electrolyte additives can modify the SEI on the negative electrode and the passivation layer on the positive electrode. Research developments about electrolyte additives will be separated into those that are thought to act at the negative electrode, and those that are thought to act at the positive electrode.

A large number of chemicals have been proposed as film forming electrolyte additives for the graphite electrode such as carbonates (e.g. vinylene carbonate,[49] vinyl ethylene carbonate,[50] fluoroethylene carbonate[51]), sulfates (e.g. ethylene sulfate[52]) and boron-based additives (e.g. trimethoxyboroxine[53]). Vinylene carbonate (VC) is the most famous electrolyte additive for lithium-ion batteries and it is being used in many commercial electrolyte compositions. Xiong et al.[5] showed that the addition of VC can help increase the coulombic efficiency (CE) and help decrease the charge and discharge endpoint capacity slippages for Li/graphite cells at 50 or 60°C by apparently forming a "better" SEI.

Compared with the efforts on studies of additives for the negative electrode interphase, the development of suitable additives for the positive electrode interphase has been limited until recently. Burns et al.[6] showed that VC is a useful additive for reducing electrolyte oxidation at the positive electrode, which results in a decrease of charge endpoint capacity slippage. Based on the requirements of high voltage chemistries, the

development of new additives is needed to replace traditional carbonate-based additives because carbonates are susceptible to oxidative decomposition beyond 4.5 V.[54,55] It has been shown by Yan et al.[56] that the addition of tris(trimethylsilyl)phosphate (TTSP) yielded a capacity retention of 90.9% after 100 cycles of $Li(Ni_{0.5}Co_{0.2}Mn_{0.3})O_2$/Li cells (3 - 4.5 V) at a 1C rate. Cresce et al.[55] used tris(hexafluoro-iso-propyl)phosphate (HFiP) to dramatically improve the capacity retention of $Li(Ni_{0.5}Mn_{1.5})O_4$/Li cells cycled between 3.5 and 4.95 V, which suggested a useful modification to the electrolyte/positive electrode interphase. However, this conclusion was challenged by recent work by Li et al.[57]

1.4.2 SOLID ELECTROLYTE INTERPHASE (SEI)

In the charged state, the electrodes in contact with the electrolyte are both thermodynamically unstable. This causes various reactions and new components on the electrode surfaces to appear. Fortunately, the formed layers, called SEI, are electronically insulating and ionically conducting, which enables Li^+ transport through the SEI films. The formation of such an interphase was first introduced by Peled[22] in 1979. The SEI layers are hard to characterize because of their sensitive chemical nature, complex manner of formation and the lack of appropriate in-situ tools.[38]

1.4.2.1 The solid electrolyte interphase (SEI) at the negative electrode

Generally, the SEI on the graphite negative electrode contains organic and inorganic compounds resulting from reacted solvent, salt or additives coming from the electrolyte. It has been proposed that the SEI closer to electrode particles mainly consists of

inorganic compounds and the SEI closer to electrolyte is dominated by organic compounds.[4,34,58]

Carbonate-based solvents are typical solvents used in lithium-ion batteries. EC is used as an example to illustrate the electrochemically induced reduction mechanism:

$$2EC + 2Li^{+} + 2e^{-} \rightarrow (CH_2OCO_2Li)_2\ (s) + C_2H_4\ (g).^{4} \quad (1.3)$$

The solid products of such possible reactions are thought to be incorporated in the SEI formed on the graphite electrode. Nie et al.[59] showed that the major products caused by the reaction of EC/$LiPF_6$ electrolyte with lithiated graphite were lithium ethylene dicarbonate ($(CH_2OCO_2Li)_2$, LEDC) and LiF. Although EC and propylene carbonate (PC) have a similar structure, they show very different interphase behavior for the graphite electrode. PC-cointercalation into graphite can result in graphite exfoliation[60] while there is no co-intercalation of most EC-based electrolytes.

Various salts in the electrolyte also affect the SEI formed on the graphite electrode. Combining NMR, FTIR and XPS experiments, Nie et al.[61] investigated the impact of different salts on formation of the SEI on binder free graphite. Six different salts (lithium bis-oxalato borate (LiBOB), lithium difluorooxalato borate (LiDFOB), lithium tetrafluorooxalato phosphate (LiTFOP), lithium bis(fluorosulfonyl) imide (LiFSI), lithium bis(trifluoromethylsulfonyl) imide (LiTFSI)) mixed with EC were studied. LEDC, the primary reduction product of EC, could be found in all of the SEI films. The SEI for all electrolytes contained LiF except for the SEI formed from the LiBOB-containing electrolyte. In addition, the SEI generated from the electrolytes containing

LiBOB or LiDFOB contained multiple oxalate-containing species such as lithium oxalate and so on.

Some electrolyte additives facilitate SEI formation by electrochemically passivating an organic film on the surface of graphite through a reduction process. This kind of additive usually has a higher reduction potential than the main solvents, which causes it to form insoluble solid reaction products prior to the reactions of the electrolyte solvents.[48] VC is known to polymerize on the lithiated graphite surface and form poly alkyl Li-carbonate species which are believed to suppress solvent and salt anion reduction.[49,62]

1.4.2.2 The passivation layer at the positive electrode

Compared with the SEI formed on the graphite surface, there has been rather limited work on the positive electrode surface because of the complicated species formed there. However, some understanding about this chemistry and electrochemistry exist, especially on high-voltage (> 4.5 V) surfaces which are very important to the development of advanced Li-ion batteries.

Based on inductively coupled plasma mass spectrometry (ICP-MS), Raman, XPS, FTIR and electron microscopy, Aurbach et al.[63] showed that some common positive electrode materials such as $LiCoO_2$, $LiMn_2O_4$ and $LiFePO_4$ could develop rich surface chemistry in alkyl carbonate solutions due to numerous reactions (e.g. acid–base reactions, nucleophilic reactions, induced polymerization). The formed surface films mainly consisted of LiF, $ROCO_2Li$, $ROCO_2M$ (M = transition metal), ROLi and polycarbonates.

Furthermore, transition metal dissolution could occur from the surface of positive electrode material.

It has been generally proposed that the interphase between positive electrode and electrolyte formed in carbonate-based electrolytes can be stabilized up to ~ 4.5 V,[64] above which sustained oxidation of electrolyte would occur.[39] Some interphase analysis on the high-voltage positive electrode material, ($LiMn_{1.6}Ni_{0.4}O_4$), by Dedryvére et al.[65] showed that only a small quantity of lithiated species were deposited on the positive electrode surface while vast amounts of organic species caused by the decomposition of solvent at high potential could be detected.

CHAPTER 2. EXPERIMENTAL TECHNIQUES

2.1 SAMPLE PREPARATION FOR ARC

This section discusses the preparation of ARC samples, including fabrication of pellet electrodes, construction of pellet cells, cell testing and construction of ARC samples.

2.1.1 PELLET ELECTRODES FOR ARC

The electrode materials of interest in this study are commercial NMC111 and mesocarbon microbead (MCMB) graphite which were obtained from 3M Company (St. Paul, MN, USA) and E-One Moli/Energy Canada Ltd. (Maple Ridge, BC), respectively. The MCMB (heated to 2650^{o}C) used was produced by Osaka Gas (Chuo-ku, Osaka, Japan), and had a probability of turbostratic misalignment of P = 0.19.[66]

Electrode preparation proceeded as follows: a mixture of active material (NMC or MCMB), Super C45 (Timcal), PVDF binder (Kynar 301F, obtained from Elf-Atochem) and N-methyl pyrrolidone (NMP) (Sigma-Aldrich, ≥ 99.0%) used to make the pellet electrode was prepared by making slurry in a small hardened steel shaker bottle. The weight ratios in the slurry for the active material, carbon black and binder were 86:7:7 and 92:4:4 for MCMB and NMC, respectively. The bottle was shaken in a low speed two-clamp laboratory mill (Spex8000-D Mixer Mill, as shown in Figure 2.1) for roughly 1 hour to mix the ingredients. The slurry was then dried in a 120°C oven overnight to fully evaporate the NMP. After dying in the oven, the powder was ground lightly in a mortar. Approximately 280 mg of the electrode powder was put in a stainless steel die to

press a pellet under a pressure of 13.8 Mpa (2000 psi). The pellet was about 13 mm in diameter and was approximately 1 mm thick, as shown in Figure 2.2.

Figure 2.1 Spex8000-D Mixer Mill: the lid of the machine is open in a) and closed in b), respectively.

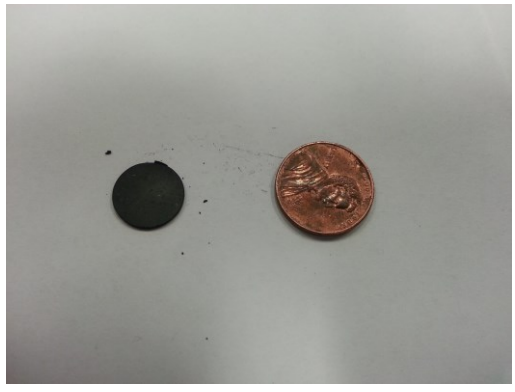

Figure 2.2 A pellet electrode compared to an American penny.

2.1.2 THE CONSTRUCTION OF PELLET CELLS

Before constructing cells, the stainless steel parts of a 2325 type coin cell (23 mm diameter, 2.5 mm thickness), the stainless steel spacer and the pellet electrodes were heated in a 90°C vaccum antechamber overnight. Cells were made in an argon-filled glove box according to the process shown in Figure 2.3. The pellet electrode was placed in the center of the positive terminal with enough electrolyte to wet the electrode. Then

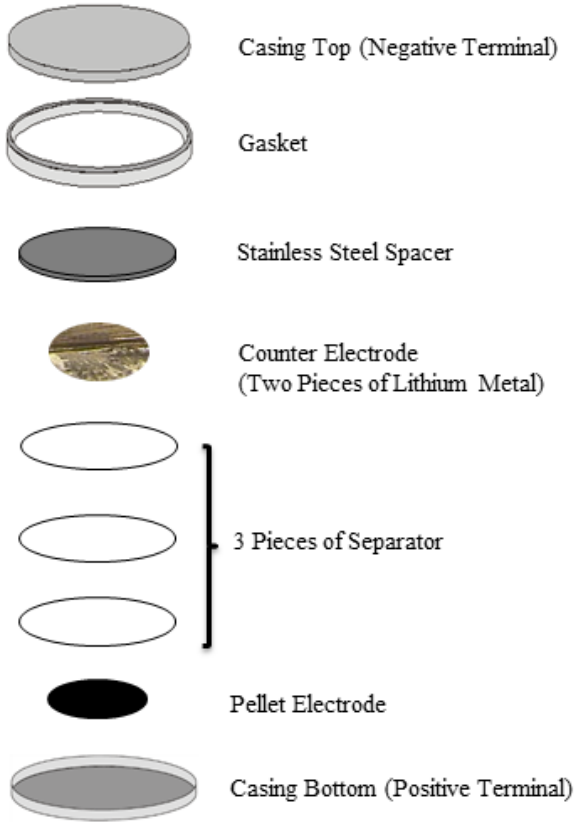

Figure 2.3 Construction of a 2325 size pellet coin cell.

three pieces of separator (Celgard 2300) were put on the pellet electrode with a little electrolyte. Once the separator became clear because of immersion in electrolyte, two pieces of lithium metal were added as the counter electrode. Then the spacer and negative terminal with gasket were placed. The cell was then placed in two sequential crimpers to be properly sealed. 1M $LiPF_6$ in EC/DEC (1/2, v/v, BASF, water content was 3.8 ppm) or 1M $LiPF_6$ in EC/EMC (3/7, wt%, BASF, water content was 12.1 ppm) was used as the control electrolyte for the construction of pellet cells described in this thesis.

2.1.3 CELL TESTING

All assembled pellet cells were placed in temperature controlled boxes (30. ± 0.1°C) and were tested using a charger obtained from E-One Moli Energy (Maple Ridge, BC, Canada). The cells were charged or discharged using a special protocol called charge signature curve (RSIG) or discharge signature curve (DSIG) in order to allow the cell to equilibrate at a particular lithium content.[11]

NMC pellet cells were first charged to 4.2 V vs. Li with a current of 1.0 mA (~ C/40) using RSIG. After reaching 4.2 V, the cells were allowed to relax under open-circuit conditions for 15 min. Then the cells were charged to 4.2 V again using half of the original current, 0.5 mA. This continued for 5 successive charges, at the end of which the current was 0.0625 mA. For MCMB pellet cells, they were discharged to 0 V vs. Li using DSIG. The DSIG procedure was same as the RSIG procedure in this study except the current direction was opposite to RSIG. After 5 successive discharges, the lithium

entered the graphite structure as much as possible. Although the C rate used for discharging MCMB pellet coin cells was different from that of charging NMC pellet coin cells, it did not affect the required lithium content of the electrode materials for this experiment.

Figures 2.4(a) and (b) show an example of a signature curve charge for NMC111 to 4.2 V while Figures 2.4(c) and (d) show an example of a signature curve discharge for MCMB to 0.0 V. The discharge time of MCMB pellet coin cell is shorter than the C rate according to the calculation below because the pellet cells have poor rate capability and MCMB is not perfect graphite.[66,67]

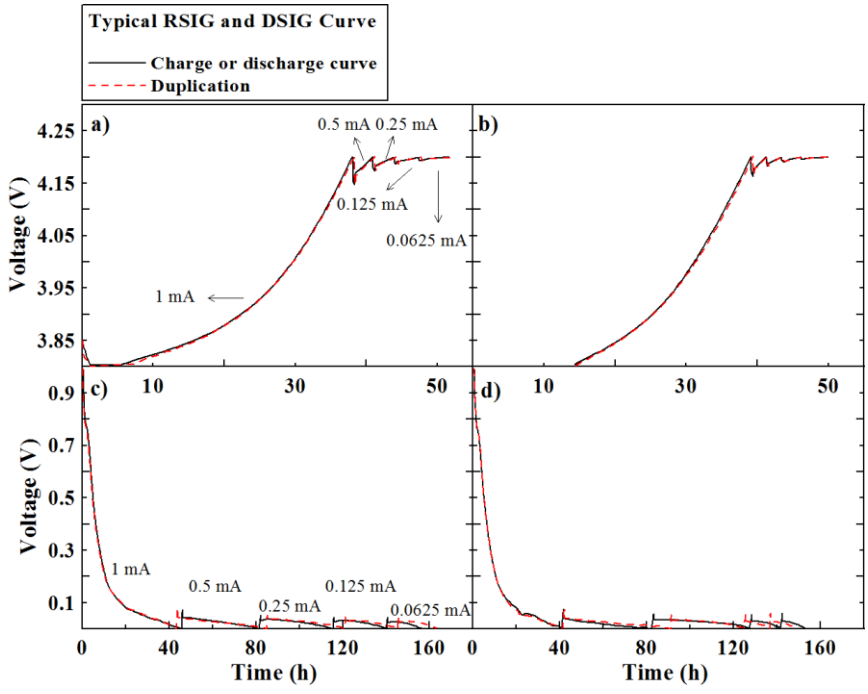

Figure 2.4 Typical charge or discharge curve for pellet coin cells: a) charge using 1M $LiPF_6$ in EC/DEC (1/2, v/v); b) charge using 1M $LiPF_6$ in EC/EMC (3/7, wt%); c) discharge using 1M $LiPF_6$ in EC/DEC (1/2, v/v); and d) discharge using 1M $LiPF_6$ in EC/EMC (3/7, wt%).

Table 2.1 shows the specific capacity and lithium content for NMC pellet cells and MCMB pellet cells, respectively, after the RSIG or DSIG test described above. The calculation of the lithium content in NMC111 and in graphite were made as described below:

a) NMC111:

Molar mass of NMC111 before charging: 6.941 g/mol + 58.693 g/mol ÷ 3 + 54.938 g/mol ÷ 3 + 58.933 g/mol ÷ 3 + 15.999 g/mol × 2 = 96.461 g/mol

Theoretical specific capacity (for 1 gram of NMC111): 1.000 g ÷ 96.461 g/mol × 96500 C/mol ÷ 3.60 C/mAh = 278 mAh

Lithium content: 1.00 - 160 (± 5) mAh/g ÷ 278 mAh/g = 0.424 ± 0.018

b) Graphite:

If perfect graphite is fully lithiated, LiC_6 will form.

The theoretical specific capacity (for 1 gram of graphite): 1.000 g ÷ (12.011 g/mol × 6) × 96500 C/mol ÷ 3.60 C/mAh = 372 mAh

Lithium content: 310 (± 10) mAh/g ÷ 372 mAh/g = 0.833 ± 0.027

Note: For MCMB with P = 0.19 the expected Li content is 1 – P = 0.81

Table 2.1 A summary of typical specific capacity and lithium content for NMC and graphite electrodes after charging or discharging.

Electrode	Typical specific capacity after test	Typical lithium content after test
$Li(Ni_{1/3}Mn_{1/3}Co_{1/3})O_2$	~ 160±5 mAh/g	$Li_{\sim 0.424}(Ni_{1/3}Mn_{1/3}Co_{1/3})O_2$
Graphite	~ 310±10 mAh/g	$Li_{\sim 0.833}C_6$

2.1.4 CONSTRUCTION OF ARC SAMPLES

The lithiated/delithiated samples with electrolyte are air-sensitive, thus ARC sample construction was performed in an argon-filled glove box. All the cells were transferred to an argon-filled glove box after the RSIG or DSIG test and then were opened using a cell opener. Then the lithiated or delithiated pellet electrodes were lightly ground with a small mortar and pestle by hand and then were rinsed using dimethyl carbonate (DMC, Sigma-Aldrich, ≥ 99.0%) to remove the original electrolyte. Previous reports have shown that the rinsing procedure changed neither the bulk structure nor the thermal behavior of the lithiated or delithiated materials.[68,69] The rinsing procedure was as follows. First, the ground powder was put into a small centrifuge tube shown in Figure 2.5(a). Then DMC was added until 2/3 of the tube was filled. The centrifuge tube was closed tightly, shaken by hand for about 40 s and placed into the centrifuge inside the glove box shown in Figure 2.5(b). The tubes were spun at 13,000 rpm for 4 min. Then DMC was decanted into a waste bottle and the rinsing procedure was repeated a total of 4 times. Then the wet powder was transferred into the vaccum antechamber for drying the powder

overnight to remove the residual DMC. Then the powder was ready to be used for ARC sample construction.

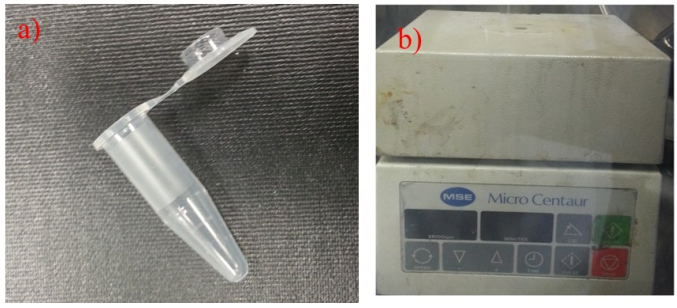

Figure 2.5(a) Centrifuge tube and (b) Micro Centaur centrifuge for rinsing the electrode powder after opening the pellet cells.

The ARC sample holder was a 0.015 mm wall, 6.35 mm diameter stainless steel tube (type 304). All the tubes were cut into 39.1 mm pieces shown in Figure 2.6 and sonicated with acetone for cleaning before they were used for ARC sample construction. One end

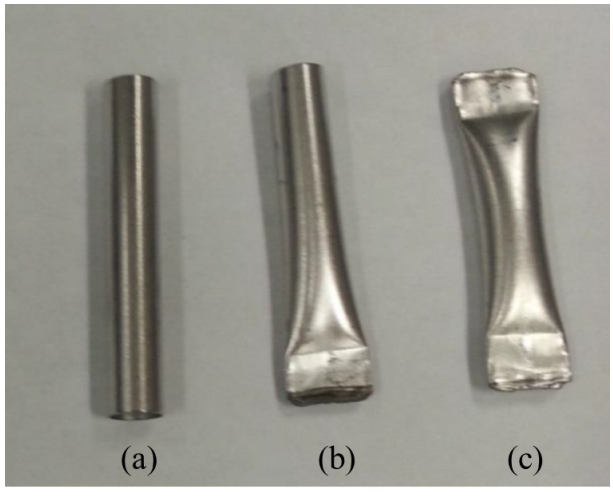

Figure 2.6 ARC test tubes at various stages of sample preparation: (a) before welding (b) welding of one end (c) after the sample was added the other end was welded closed.

of the holder was flattened and then placed into a copper welding block shown in Figure 2.7. The block had a ~ 0.2 mm gap at the top, thus the flattened end of the holder protruded out for welding. Tungsten Inert Gas (TIG) welding was used because it did not contaminate the glove box environment nor increase the ARC holder mass. A Miller Maxstar 91 ARC welder with a Snap Start II high frequency ARC starter was used. Once one end of the ARC holder was sealed, a certain amount of lithiated/delithiated powder or electrolyte was added to it. Then the other end of the holder was welded closed.

Well-sealed ARC holders were taken out of the glove box and were sonicated for 20 min to ensure mixing between the powder and electrolyte. Then a small piece of stainless steel connecting tab was attached to the ARC sample holder using a spot welder to make a small "pocket". The pocket was used to hook the ARC holder to the thermocouple of the ARC machine for the test. Finally the ARC sample was ready for testing.

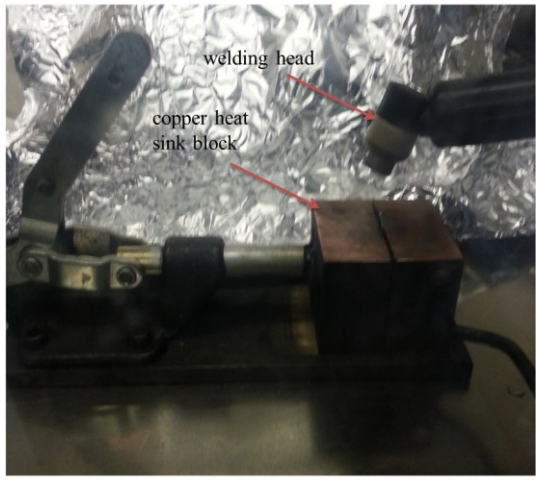

Figure 2.7 Welding head and copper heat sink block used for welding during the preparation of ARC samples.

2.2 THEORY OF ACCELERATING RATE CALORIMETRY

Since the information which can be obtained from adiabatic calorimetry, such as ARC, consists of both thermodynamic and kinetic information,[70] it is necessary to illustrate the basic theory of ARC from both kinetic and thermodynamic aspects.

Based on physical chemistry and MacNeil's previous work,[70,71] a single-step thermally induced reaction rate of the conversion of reactants to products can be written as the following:

$$\frac{d\alpha}{dt} = k(T)f(\alpha) \qquad \text{(Equation 2.1)}$$

In equation 2.1, t is the time, T is the absolute temperature (in Kelvin) and α is the fractional degree of conversion of reactants ($0 \leq \alpha \leq 1$) to products. It is common to interpret the temperature dependant rate constant k(T) using the Arrhenius equation as the following:

$$k(T) = Ae^{-E_a/RT} \qquad \text{(Equation 2.2)}$$

where E_a is the activation energy, A is the pre-exponential factor, T is the absolute temperature (in Kelvin) and R is the universal gas constant. Table 2.2 shows some examples of the reaction model, f(α), found for the thermal decomposition of solids under different physical situations.[72] The shape of the self-heating rate versus temperature curve for ARC experiments is very sensitive to the choice of f(α).[70]

Table 2.2 Reaction models applied to describe the thermal decomposition of solids.[70,72]

Reaction Model			$\frac{d\alpha}{dt}=k\alpha^m(1-\alpha)^n(-\ln(1-\alpha))^p$		
			m	n	p
1	One-dimensional diffusion	$k\alpha^{-1}$	-1	0	0
2		$k\alpha$	1	0	0
3	Power law	$k\alpha^{1/2}$	0.5	0	0
4	Power law	$k\alpha^{2/3}$	0.6667	0	0
5	Power law	$k\alpha^{3/4}$	0.75	0	0
6	Zero order	k	0	0	0
7	Contracting sphere	$k(1-\alpha)^{2/3}$	0	0.6667	0
8	Contracting cylinder	$k(1-\alpha)^{1/2}$	0	0.5	0
9	First order (n^{th} order)	$k(1-\alpha)$	0	1	0
10	Second order (n^{th} order)	$k(1-\alpha)^2$	0	2	0
11	Avrami-Erofeev	$k(1-\alpha)(-\ln(1-\alpha))^{1/2}$	0	1	0.5
12	Avrami-Erofeev	$k(1-\alpha)(-\ln(1-\alpha))^{2/3}$	0	1	0.6667
13	Avrami-Erofeev	$k(1-\alpha)(-\ln(1-\alpha))^{3/4}$	0	1	0.75
14	Autocatalytic	$k\,\alpha\,(1-\alpha)$	1	1	0
15	Two-dimensional diffusion	$k(-\ln(1-\alpha))^{-1}$	0	0	-1
16	Diffusion controlled	$k(1-(1-\alpha)^{1/3})^{-1}-(1-\alpha)^{2/3}$			
17	Diffusion controlled	$k((1-\alpha)^{-1/3}-1)^{-1}$			

Based on the previous work of MacNeil et al.,[70,71] the self-heating rate observed in ARC experiments is given as the following equation:

$$\frac{dT}{dt} = \frac{h}{C_{tot}} \times \frac{d\alpha}{dt} \quad \text{(Equation 2.3)}$$

where h is the total heat produced due to the reaction (J) and C_{tot} is the total heat capacity of the reactants and the sample bomb (J/K). In order to illustrate the relationship between h/C_{tot} and temperature rise (ΔT), more equations are used:

$$\int_0^{\infty} \frac{dT}{dt} dt = \Delta T \quad \text{(Equation 2.4)}$$

$$\int_0^{\infty} \frac{h}{C_{tot}} \frac{d\alpha}{dt} dt = \frac{h}{C_{tot}} \Delta\alpha \quad \text{(Equation 2.5)}$$

$\Delta\alpha = 1$ (when the reactants are consumed completely) (Equation 2.6)

Thus $\Delta T = \frac{h}{C_{tot}}$ (Equation 2.7)

Combining equations 2.1, 2.3 and 2.7, the following equation can be used for the self-heating rate versus temperature:

$$\frac{dT}{dt} = \Delta T k(T) f(\alpha) \quad \text{(Equation 2.8)}$$

Equation 2.8 can be converted to the following equation when the natural logarithm of both sides is taken with the combination of equation 2.2.

$$\ln\left(\frac{dT}{dt}\right) = \ln[\Delta T k(T) f(\alpha)] = \ln\left(A\Delta T f(\alpha)\right) - \frac{E_a}{RT} \quad \text{(Equation 2.9)}$$

There will be an example of a simulation of ARC profiles using these equations shown in the next part of this thesis.

2.3 INTRODUCTION TO THE ACCELERATING RATE CALORIMETER

2.3.1 GENERAL CONSTRUCTION OF THE MACHINE

The accelerating rate calorimeter, initially developed by the Dow Chemical Company and then modified by Columbia Scientific Industries,[73] is a good choice for hazard evaluation of reactive chemicals.

A schematic of the accelerating rate calorimeter is shown in Figure 2.8. Some heaters are embedded in different zones (top, side and bottom) of a large nickel-plated, copper container called the "jacket" here. Furthermore, some temperature sensors are distributed in different places near the heaters around the jacket.

The sample tube, which is in the center of the container, is hooked on the sample temperature sensor (type-N thermocouple) which is referenced to an ice point reference. During the test, if there is some heat released by the sample tube because of an exothermic reaction, a temperature difference between the jacket and the sample tube will be detected. Then the jacket will be heated to match the jacket temperature to the sample temperature. Therefore there is no heat flow between the sample tube and the jacket, which assures adiabatic conditions for the sample. The time-temperature behavior of the sample is recorded during the runaway process.

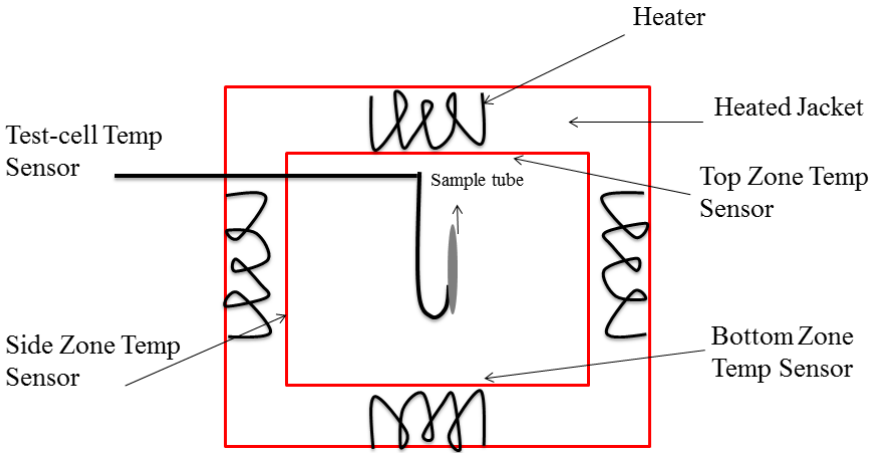

Figure 2.8 Schematic of an Accelerating Rate Calorimeter.

Figure 2.9 shows the opening of the blast shell of an ARC machine. In Figure 2.9(a), the power management module (PMM) controls the power to the jacket heater with commands from the processor unit while the calorimeter support module (CSM) mainly contains the control valve for cooling air.[74] The blast shell shown in Figure 2.9(b) is a further protection in case of accidents because the ARC can be used for research about thermal instability of explosives.[73]

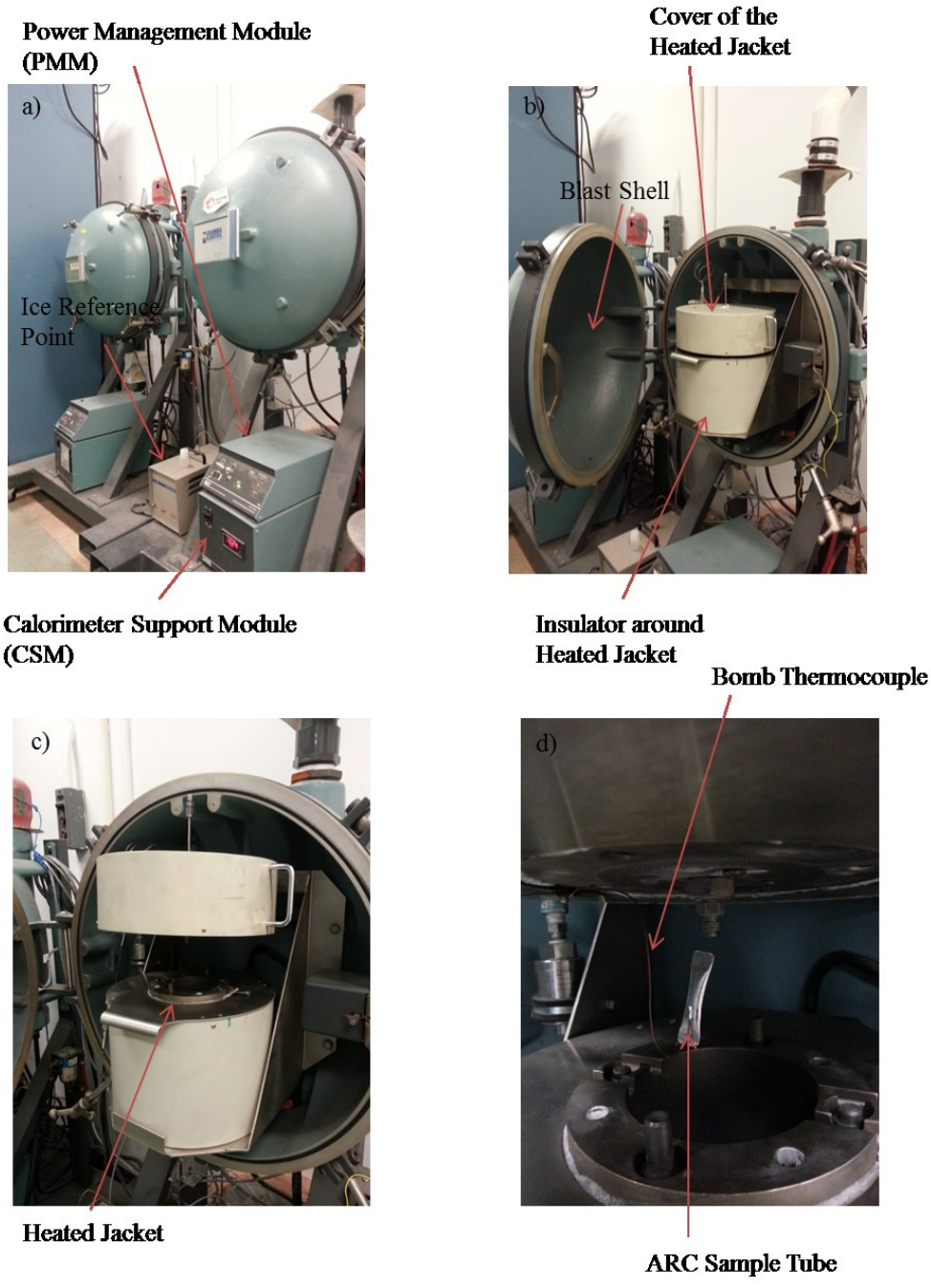

Figure 2.9 (a)-(d) The process of opening the ARC during which different parts of the machine are shown.

2.3.2 ANNEAL AND CALIBRATION MODE

The anneal mode on the ARC is important because it allows the thermocouple to correct changes and instabilities in response which result from the damage to the oxide layer or crystal structure changes of the thermocouple. Therefore, it is necessary to do an anneal run after replacing or straining a thermocouple.

In the anneal run, the instrument is programmed to control the calorimeter temperature to a constant temperature (425°C for this thesis).[74] Then it should be held at least 12 hours at this temperature (425°C for this thesis) and be stopped and cooled manually.

The calibration mode is also an important mode for the ARC because it helps compensate slight sensitivity differences between the bomb thermocouple and the jacket thermocouples. In the calibration mode, the instrument chooses a set point temperature and controls the jacket temperature to this value. The heating rate is determined by the user, usually 10°C/min. The bomb is allowed to stabilize during a wait time and then several measurements of the bomb temperature are averaged. Through the comparison between the averaged bomb temperature and the jacket temperature, an offset value in microvolts for the bomb thermocouple can be determined for this set-point temperature.[74] In order to get the corrected bomb temperature, which equals the jacket temperatures, the offset value should be added to the bomb temperature.

The offsets are evaluated usually from 50°C to 375°C in 10°C steps, which is wider than the temperature range of the real sample tests. Figure 2.10 shows a typical calibration curve, offset value vs. temperature. In this profile, the offsets vary smoothly with

temperature and do not change more than about ± 10 mV from one 50°C temperature increment to the next. Also the highest offset value is below 100 mV, which indicates an acceptable calibration curve.[74]

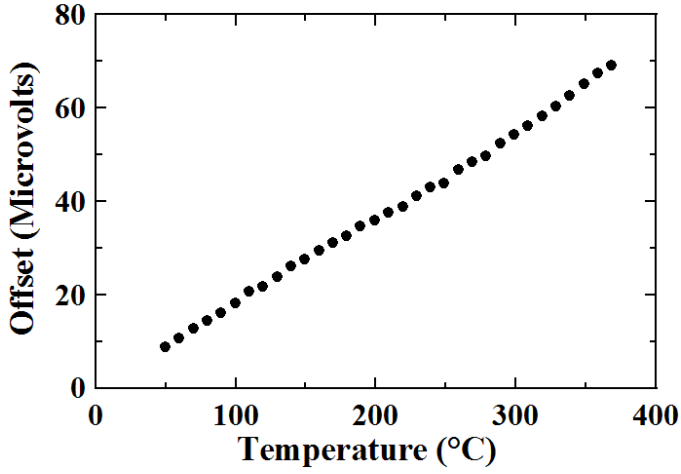

Figure 2.10 A typical example of a calibration curve for an ARC.

2.3.3 HEAT/WAIT/SEARCH MODE AND STANDARD TEST

After the thermocouple has been calibrated, the ARC is ready to do normal measurements. Usually Heat-Wait-Search (HWS) mode was used for testing. In HWS mode, the jacket is heated to an initial temperature, then waits for an equilibration period so that the sample temperature approaches that of the jacket. After the equilibration period, the self-heating rate of the sample is measured. If the self-heating rate is greater

than or equal to the set sensitivity (0.03°C/min in this thesis) then the ARC considers an exotherm to be detected.

If an exotherm is detected, the self-heating rate of the sample will be tracked in exotherm mode. If not, the jacket will be heated to the next temperature step. In HWS mode, the jacket and the sample are stepped up from the starting temperature to the end point temperature if the self-heating rate of the sample does not exceed the set safety limit of the ARC (20°C/min for this thesis). Once the self-heating rate exceeds the safety limit, the heating is stopped and the cooling mode is initiated automatically.

In order to test the instrument and the ARC sample construction, di-tert-butyl peroxide (DTBP), a chemical widely studied as a cetane improver in diesel fuels,[75] was chosen as a standard chemical to be run in the ARC because of its simple decomposition reaction.[76] Figure 2.11 shows the chemical structure of DTBP.

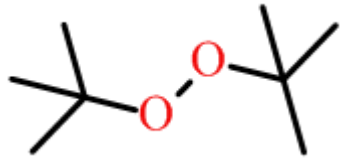

Figure 2.11 Chemical structure of di-tert-butyl peroxide (DTBP).

0.05 g of DTBP was placed in the stainless steel tube shown in Figure 2.6 using the sample construction method described before. After that, the HWS mode was used to increase the sample temperature and track the self-heating rate of the sample.

Figures 2.12(a) and (b) show the temperature versus time profile for 50 mg DTBP measured using HWS mode. The parameters for this experiment were: starting temperature was 50°C, the slope sensitivity was 0.03°C/min, the stop temperature was 350°C and the temperature step was 10°C. When the experiment began, both the jacket and the sample tube were initially heated up to the starting temperature (50°C) as shown in Figure 2.12(b). Then the machine was held for a period of time for thermal equilibrium to be achieved before search mode was performed. If the self-heating rate (SHR) was lower than the set slope sensitivity (0.03°C/min), the ARC proceeded automatically to the next HWS step until SHR higher than set slope sensitivity was detected. If the SHR was higher than 0.03°C/min, the computer-controlled jacket tracked the exothermic reaction under adiabatic conditions. The process continued until the end temperature (350°C).

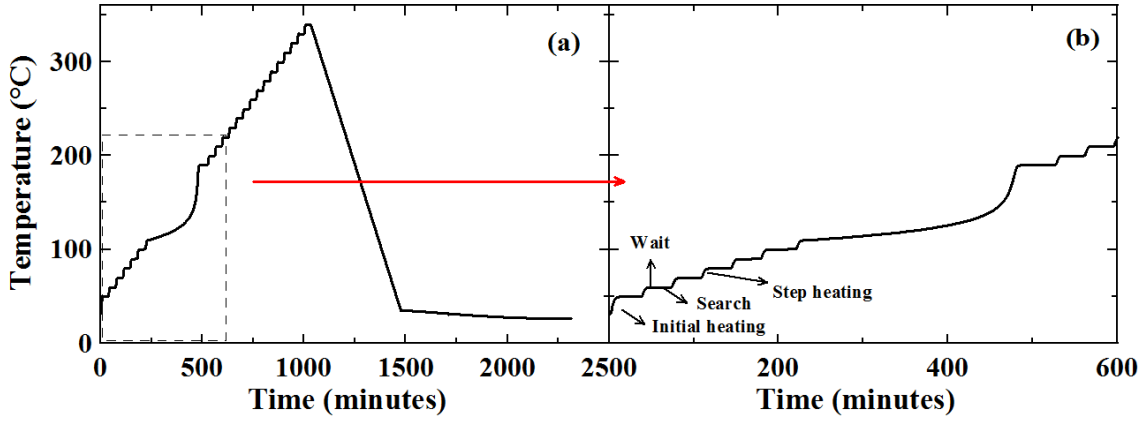

Figure 2.12 Temperature versus time profile for ARC results of DTBP. Figure 2.12(b) enlarges part of Figure 2.12(a) as indicated using the dashed line.

Figures 2.12(a) and (b) show that a SHR above 0.03°C/min was detected at around 100°C, which matches the results shown in Figure 2.13. Figure 2.13 shows the self-heating rate versus temperature for the DTBP sample. In Figure 2.13, the SHR was larger than 0.03°C/min at around 100°C. The ARC tracked the exothermic reaction at this point until the depletion of DTBP reactant inside the tube at around 190°C. The two downward spikes shown around 130°C are the result of sequential expansion of the two ends of the sample tube according to Jiang's previous work.[71]

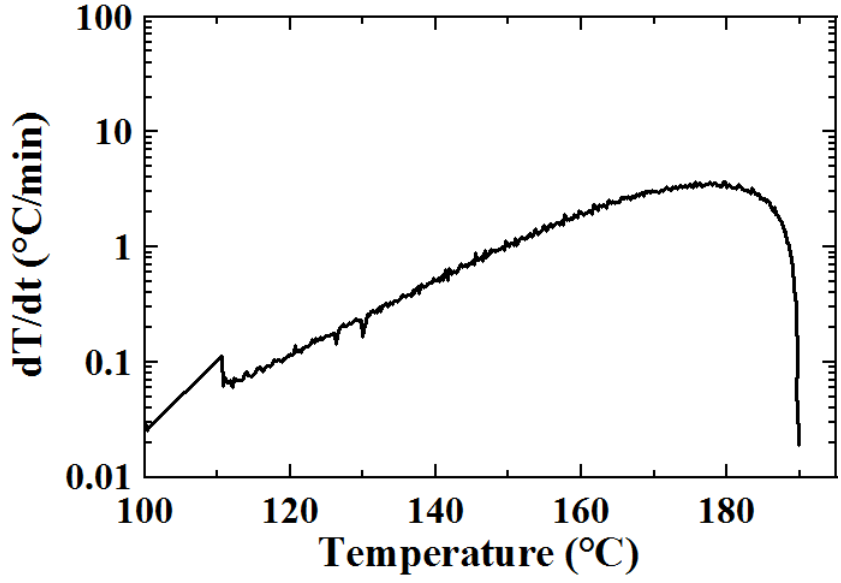

Figure 2.13 Self-heating rate versus temperature profile for the DTBP test using ARC.

Since the decomposition of DTBP is known to be a first-order reaction,[77] simple calculations were performed mainly using equations 2.1 - 2.9 and reaction model 9 in Table 2.2 shown in section 2.2.1 in order to simulate the ARC profile. The ARC result in Figure 2.13 was fitted as shown in Figure 2.14 by the red dashed line in order to extract the activation energy (E_a) and pre-exponential factor (A).

To avoid some noisy points, the parameters for the fitting were chosen as following: the temperature range was from 110°C to 190°C ($\Delta T = 80K$) and α_0 was taken to be 0.0001.

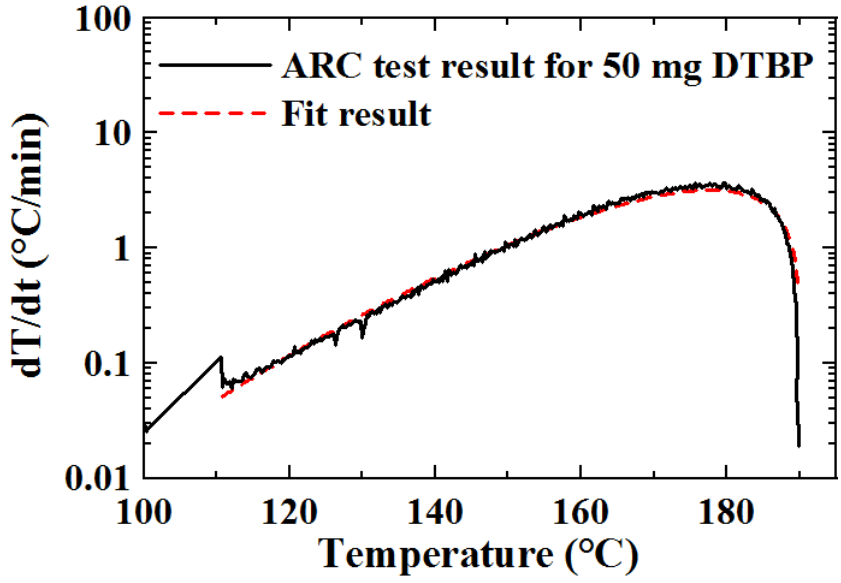

Figure 2.14 Self-heating rate versus temperature for 50 mg DTBP (black solid line) and fitted result (red dashed line).

From the fitted curve, the activation energy was determined to be about 127 kJ/mol and the pre-exponential factor (A) was around 1.29×10^{14} min^{-1}, which are close to literature values[76,77] (In the literature, E_a is between 113.2 to 158.3 KJ/mol and the order of magnitudes for A are between 10^{12} and 10^{18} min^{-1}). Figure 2.14 shows that ARC can be used for characterizing the chemical reactions using the stainless steel tube sample holders shown in Figure 2.6. Thus, in this thesis the DTBP test was used as a standard test after every calibration in order to make sure the ARC machines were in good condition.

2.4 SURFACE AREA MEASUREMENT

At a certain partial pressure and temperature, gas will form a monolayer on the surface of a solid. Based on this principle of the single-point Brunauer-Emmett-Teller (BET) surface area measurement, the surface area of a solid can be obtained by counting the number of adsorbed molecules.[78] In this thesis, a Micromeritics Flowsorb II 2300 surface area analyzer (Figure 2.15) was used for the BET surface area test on both NMC111 and graphite samples.

Before testing, calibration was performed by introducing a known quantity of N_2 gas through a septum on the analyzer and into the inline gas flow using a syringe. During the experiment, the samples were placed in U-shape air-tight glass tubes, carefully weighed, then degased at 150°C under a flow of N_2/He (3/7, v/v) mixture for 1.5 ~ 2 h. Then the glass tube containing samples was submerged in a bath of liquid N_2 for adsorption and was immersed in a bath of tap water for desorption at room temperature after full adsorption. The final results for surface area were obtained using the desorption data of the single-point BET measurement.

Figure 2.15 Micromeritics Flowsorb II 2300 surface area analyzer.

2.5 SCANNING ELECTRON MICROSCOPY (SEM)

To obtain the morphology of the materials used for the ARC studies, SEM images were taken for both NMC111 and MCMB samples. All SEM images were taken using a Phenom G2-Pro desktop scanning electron microscope (Figure 2.16) with an accelerating voltage of 5 kV and an emission current of 1.2 nA. A few milligrams of powder (MCMB or NMC) were mounted onto a SEM sample stub by pressing the powder onto carbon tape on the stub.

Figure 2.16 Phenom G2-Pro desktop scanning electron microscope.

CHAPTER 3. AN EXPLORATION OF SEVERAL FACTORS THAT MAY AFFECT ARC RESULTS

This thesis will compare the effects of some typical electrolyte additives or combinations of additives on the reactivity between charged electrode materials and electrolyte at elevated temperatures. Every experimental procedure is kept the same except for the addition of different electrolyte additives in the ARC tubes. Some experimental details need to be amplified here for completeness. Two percent VC as electrolyte additive is used as an example to illustrate the procedures used.

3.1 RINSING PROCEDURE FOR ELECTRODES TO BE STUDIED BY ARC

The rinsing procedure[79] described in the previous chapter was used to remove the original electrolyte from the charged electrode powder. It is important to determine the effect of the rinsing because rinsing was also used in this thesis. The following section illustrates the effect of the rinsing procedure on typical ARC results. The NMC pellet cells and graphite pellet cells were charged or discharged using 1M $LiPF_6$ in EC/DEC (1/2 v/v) with 2 wt% VC.

Figure 3.1 shows the self-heating rate vs. temperature for 94 mg delithiated NMC reacting with 30 mg 1M $LiPF_6$ in EC/DEC (1/2 v/v) with 2 wt% VC. There is almost no difference between the data for the rinsed and unrinsed samples.

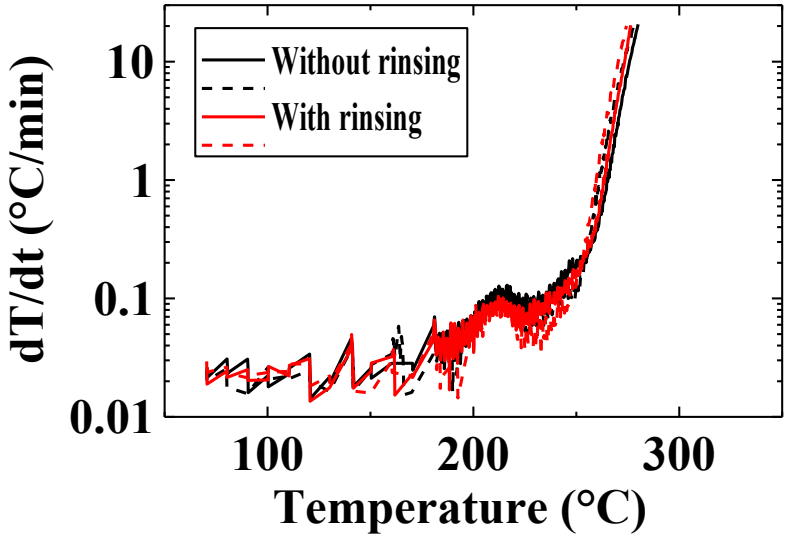

Figure 3.1 Self-heating rate vs. temperature for 94 mg delithiated NMC reacting with 30 mg 1M $LiPF_6$ in EC/DEC with 2 wt% VC.

Figure 3.2 shows the self-heating rate vs. temperature for 140 mg lithiated graphite reacting with 140 mg 1M $LiPF_6$ in EC/DEC (1/2 v/v) with 2 wt% VC. Figure 3.2 indicates that rinsing procedure has a small effect on the thermal performance of the lithiated graphite powder reacting with electrolyte.

The exothermic peak around 100°C caused by the decomposition of the metastable SEI[11] is not observed when the sample is not rinsed by DMC. After rinsing, a small peak near 100°C is observed, suggesting that the rinsing modified the SEI to a small degree. However, the positive effect of VC on the ARC performance of lithiated graphite can still be detected compared to control electrolyte even if the powder was rinsed.

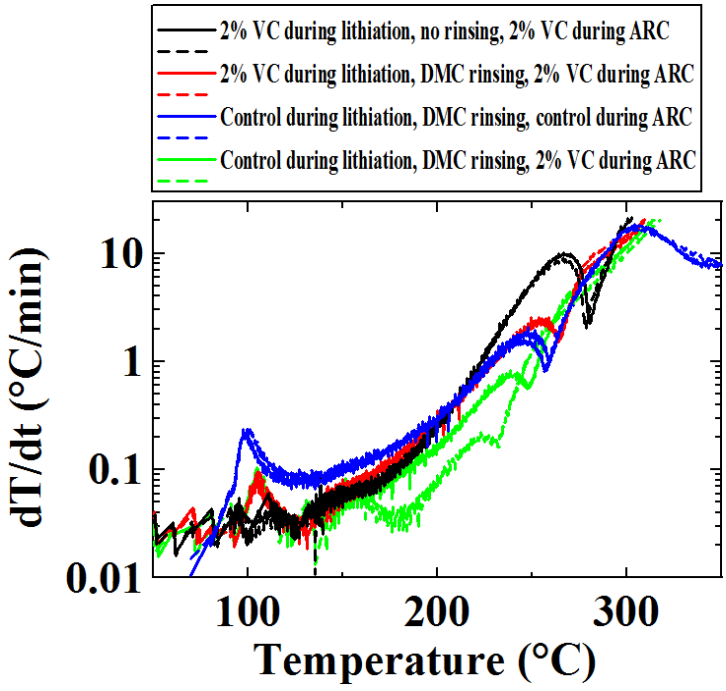

Figure 3.2 Self-heating rate vs. temperature for 140 mg lithiated graphite reacting with 140 mg 1M $LiPF_6$ in EC/DEC with or without 2 wt% VC.

3.2 THE CHOICE OF ELECTROLYTE FOR CHARGING OR DISCHARGING PELLET CELLS

In this thesis, control electrolyte (1M $LiPF_6$ in EC/DEC (1/2 v/v) or 1M $LiPF_6$ in EC/EMC (3/7 wt%)) was chosen to charge or discharge pellet cells. Additives were believed to still affect the reactivity of the charged electrodes even if they were not included in the pellet cells. In order to compare the effect of different electrolytes for charging or discharging pellet cells on ARC performance, 2% VC-containing electrolyte

was selected and compared with the results of control electrolyte. All the powders here were rinsed by DMC after the pellet cells were charged or discharged.

Figure 3.3 shows the self-heating rate vs. temperature for 94 mg delithiated NMC reacting with 30 mg 1M $LiPF_6$ in EC/DEC (1/2 v/v) with 2 wt% VC. The black curves show the results for powder charged in control electrolyte while the red curves show the results for powder charged in 2% VC-containing electrolyte. There is almost no difference between the red and black curves.

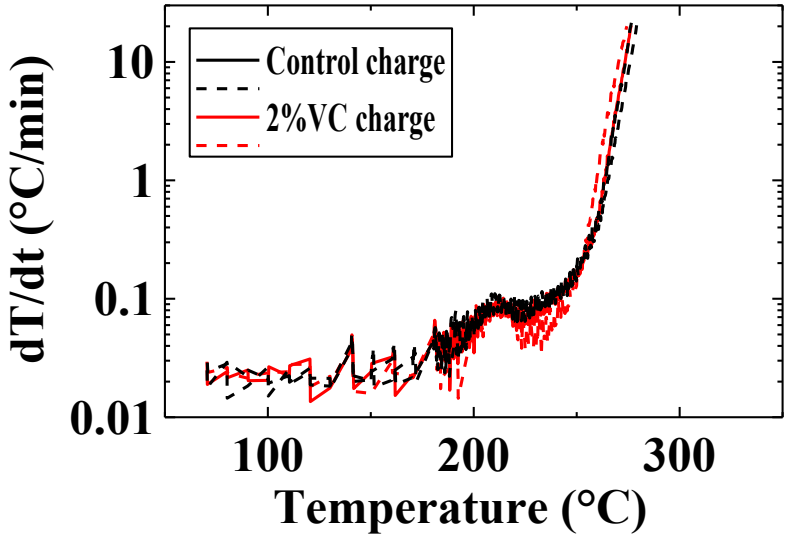

Figure 3.3 Self-heating rate vs. temperature for 94 mg delithiated NMC reacting with 30 mg 1M $LiPF_6$ in EC/DEC with 2 wt% VC. Control electrolyte is 1M $LiPF_6$ in EC/DEC (1/2 v/v).

Figure 3.4 shows self-heating rate vs. temperature for 140 mg lithiated graphite reacting with 140 mg 1M $LiPF_6$ in EC/DEC (1/2 v/v) with 2 wt% VC. There is almost no difference between the control and 2% VC discharged samples up to 150°C, especially in

the peak caused by the decomposition of metastable SEI at ~ 100°C. One of the two control discharged samples had an anomalously low SHR above 150°C.

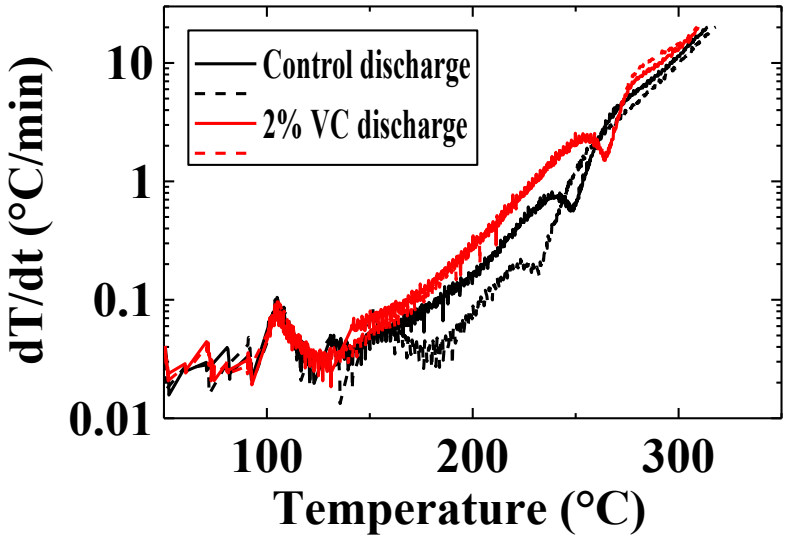

Figure 3.4 Self-heating rate vs. temperature for 140 mg lithiated graphite reacting with 140 mg 1M $LiPF_6$ in EC/DEC with 2 wt% VC.

3.3 THE EFFECT OF ADDITIVES ON THE ELECTROLYTES DURING ARC TEST

The introduction of the electrolyte additives in the carbonate-based solvents themselves might affect the thermal stability of the electrolyte itself. The self-heating rate of 0.07 g (± 3%) 1M $LiPF_6$ in EC/DEC (1/2 v/v) with selected additives (VC, FEC and PES) is shown in the following figures.

Figure 3.5 shows the self-heating rate vs. temperature for 70 mg 1M $LiPF_6$ in EC/DEC (1/2 v/v) with 2 wt% PES (a), 2 wt% FEC (b) and 2 wt% VC (c) compared with control electrolyte (1M $LiPF_6$ in EC/DEC). Exothermic reactions can be observed mainly in two

temperature ranges with or without electrolyte additives. The first was around 200°C and the second was around 320°C. The self-heating rates observed in any of the electrolyte samples were very low, less than 0.3°C/min. The additives had virtually no effect on the SHR versus temperature profiles.

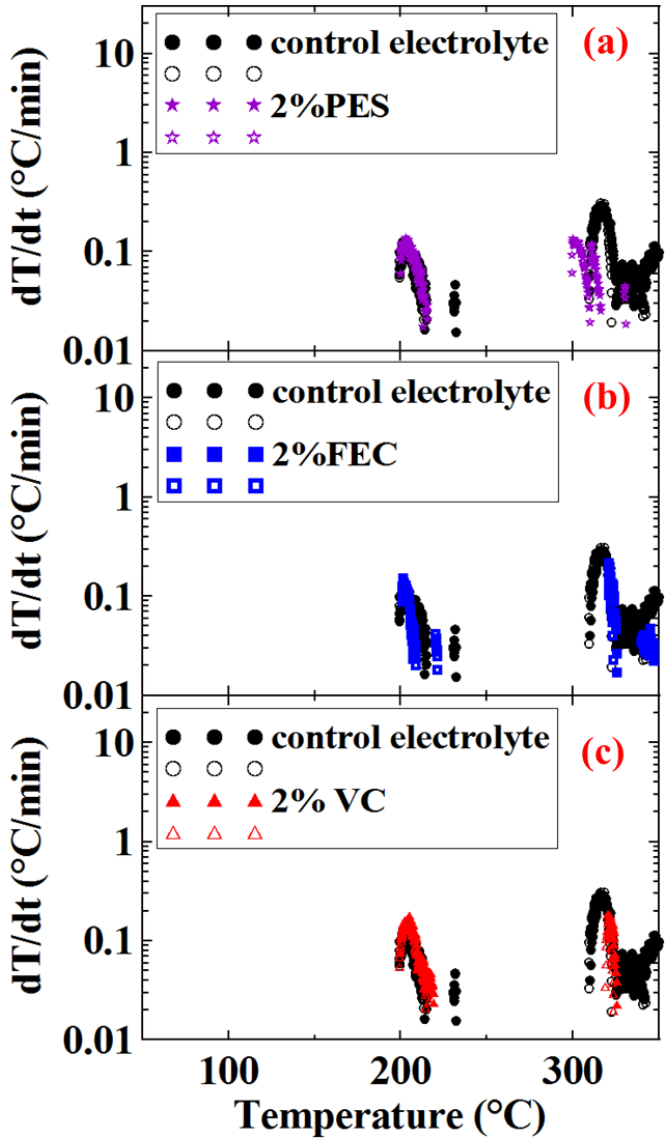

Figure 3.5 Self-heating rate vs. temperature for 70 mg 1M $LiPF_6$ in EC/DEC with 2 wt% PES (a), 2 wt% FEC (b) and 2 wt% VC (c) compared to control electrolyte.

CHAPTER 4. SAFETY STUDY OF ADDITIVES USING ARC

This chapter presents results obtained using ARC using the methods discussed in Chapters 2 and 3. Section 4.1 presents the results of the impact of some traditional electrolyte additives, VC, fluoroethylene carbonate (FEC) and vinyl ethylene carbonate (VEC), on electrode/electrolyte reactivity. Section 4.2 presents the results of ARC studies made on delithiated NMC or lithiated graphite, respectively, using some promising sulfur-containing and phosphorus-containing additives. Section 4.2 explores the effects of all these additives on the thermal performance at the level of 2 wt%. Section 4.3 presents the results of a comparative study of the effects of some additive combinations. These additive combinations show better capacity retention during charge-discharge cycling, and produce less gas during cycling than single additives.

4.1 THE IMPACT OF VINYLENE CARBONATE, FLUOROETHYLENE CARBONATE AND VINYL ETHYLENE CARBONATE ELECTROLYTE ADDITIVES ON ELECTRODE/ELECTROLYTE REACTIVITY

4.1.1 EXPERIMENTAL

Pellet cells and ARC samples were made following the procedure described in Chapter 2. Figures 4.1(a) and (b) show SEM micrographs of the graphite (MCMB) and NMC particles used for this study, respectively. The MCMB particles have spherical shape and are of relatively uniform size with a diameter around 20 μm. The size of the spherical NMC particles is less uniform with a diameter range from ~ 5 μm to ~ 20 μm. The single-point BET surface areas of the graphite (MCMB) and NMC powders were 0.30 ± 0.01 m^2/g and 0.48 ± 0.01 m^2/g, respectively, as measured with a Micromeritics Flowsorb 2300 instrument.

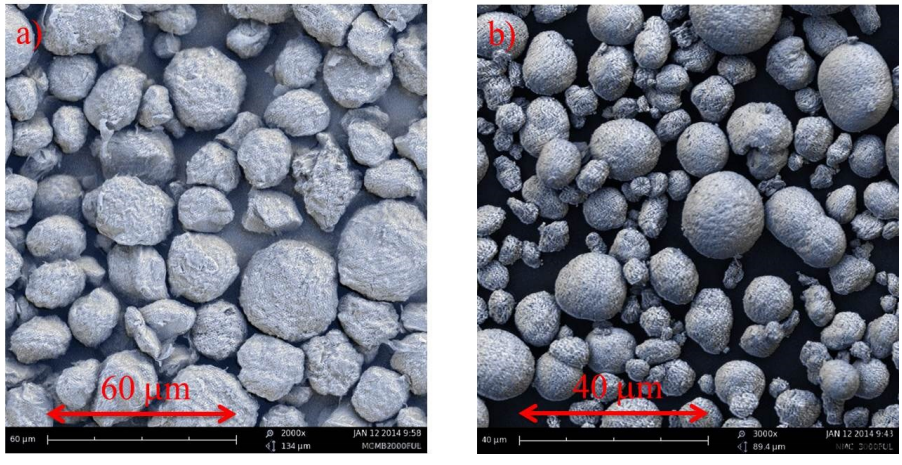

Figure 4.1 SEM images of the graphite (MCMB) (a) and NMC (b) used.

Charged electrode materials and electrolyte containing various concentrations vinylene carbonate (VC, BASF, 99.97%), fluoroethylene carbonate (FEC, BASF, 99.94%) and

vinyl ethylene carbonate (VEC, BASF, 99.9%), were put in the ARC tubes for the test. Figure 4.2 shows the chemical structures of VC, FEC and VEC.

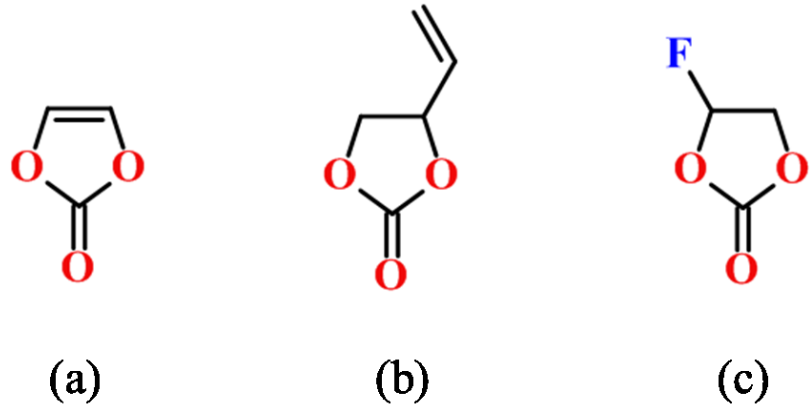

Figure 4.2 Chemical structures of the electrolyte additives used (a) vinylene carbonate (VC) (b) vinyl ethylene carbonate (VEC) and (c) fluoroethylene carbonate (FEC).

4.1.2 RESULTS AND DISCUSSION

Figures 4.3(a), (b) and (c) show the SHR versus temperature for 94 mg delithiated NMC with 30 mg 1M $LiPF_6$ in EC/DEC containing 10 wt% VC, VEC or FEC tested between 70°C and 350°C. The results for duplicate samples are given as dashed lines in each panel to demonstrate the repeatability of these experiments. A 10 wt% loading of the additive was used initially in order to allow detection of the impact of the additives using ARC. Generally, compared to the control electrolyte, VC, VEC and FEC do not have a strong impact on the SHR versus temperature of charged NMC in electrolyte. However, there are still some differences between the three additives. Panel (a) shows that 10 wt% VC and control electrolyte had virtually the same response. Panel (b) shows that the onset temperature of the exotherm for samples with 10 wt% VEC was around 160°C,

which was lower than that of the samples with control electrolyte. Panel (c) shows that the sample with 10 wt% FEC had lower reactivity than the control sample in the temperature range between 210°C to 220°C. Figure 4.3 shows that almost all of the samples exceeded the maximum tracking rate of the ARC before 275°C. The samples that did not exceed the maximum tracking rate, reached close to 20°C/min and such variations between nominally identical samples are common in ARC experiments.

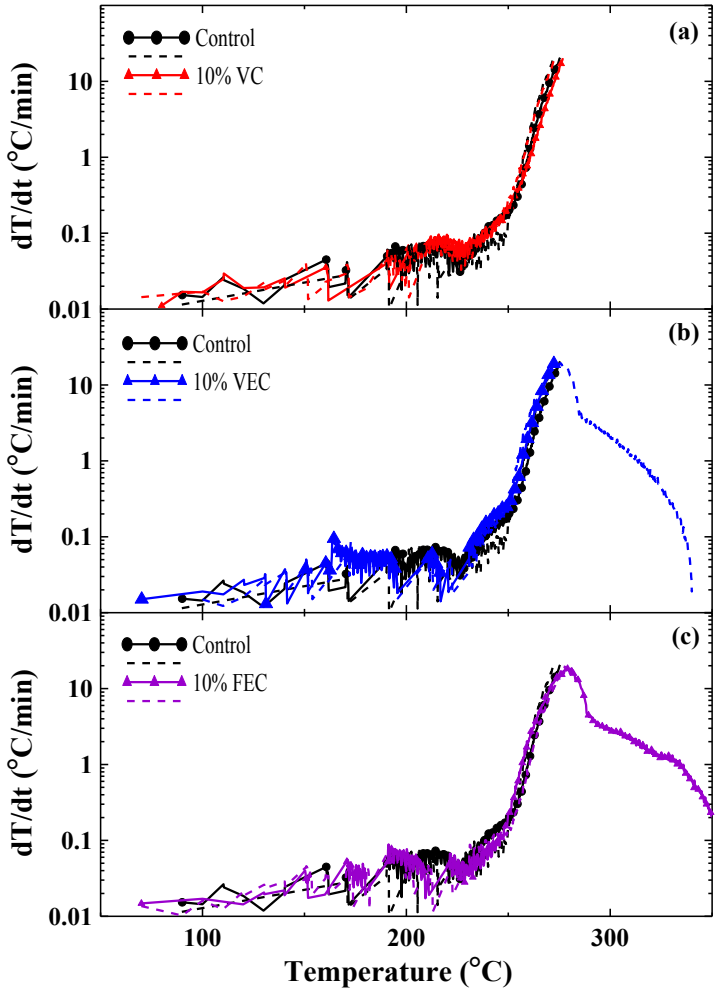

Figure 4.3 Self-heating rate vs. temperature for delithiated NMC reacting with 1M $LiPF_6$ in EC/DEC with 10 wt% VC (a), with 10 wt% VEC (b) or with 10 wt% FEC (c) compared with the control electrolyte.

Figure 4.4(a) shows the SHR versus temperature results for 70 mg lithiated graphite heated with 70 mg 1M $LiPF_6$ in EC/DEC containing 10 wt% VC between 80°C and 350°C. Unlike delithiated NMC, lithiated graphite showed quite different reactivity in electrolytes containing VC or FEC compared to samples with control electrolyte. The impact of these additives was mainly in the temperature range between 80°C and 200°C, indicated in the dashed frames in Figure 4.4(a), (b) and (c). Figure 4.4(a) shows that 10 wt% VC helped suppress the exothermic peak around 100°C and decreased the SHR in the temperature range between 80°C and 150°C. According to the report from Richard et al.,[11] the exothermic peak around 100°C can be ascribed to the decomposition of metastable SEI components. Therefore, the suppression of this peak suggests a much more thermally stable SEI formed in the presence of VC, which agrees well with previous reports.[5,49,62] Richard[11] also showed that the second exothermic process appearing after the first peak is caused by the reaction of intercalated Li with solvent to form a new SEI. Figure 4.4(a) shows that the SHR increased in the temperature range between 180°C and 250°C in the presence of 10 wt% VC.

Figure 4.4(b) shows the SHR versus temperature for 70 mg lithiated graphite heated with 70 mg 1M $LiPF_6$ in EC/DEC containing 10 wt% VEC additive. The results indicate that VEC does not have an obvious influence on the SHR of lithiated graphite. Figure 4.4(c) shows the SHR versus temperature for 70 mg lithiated graphite heated with 70 mg 1M $LiPF_6$ in EC/DEC containing 10 wt% FEC additive. The results demonstrate that FEC increased the thermal reactivity of lithiated graphite in electrolyte because the onset temperature occurred at a lower temperature, near the starting temperature of the ARC experiment, than that of the control samples. As in the case of VC, the reactivity of the

10 wt% FEC samples was greater than the control sample in the range between 160°C and 250°C.

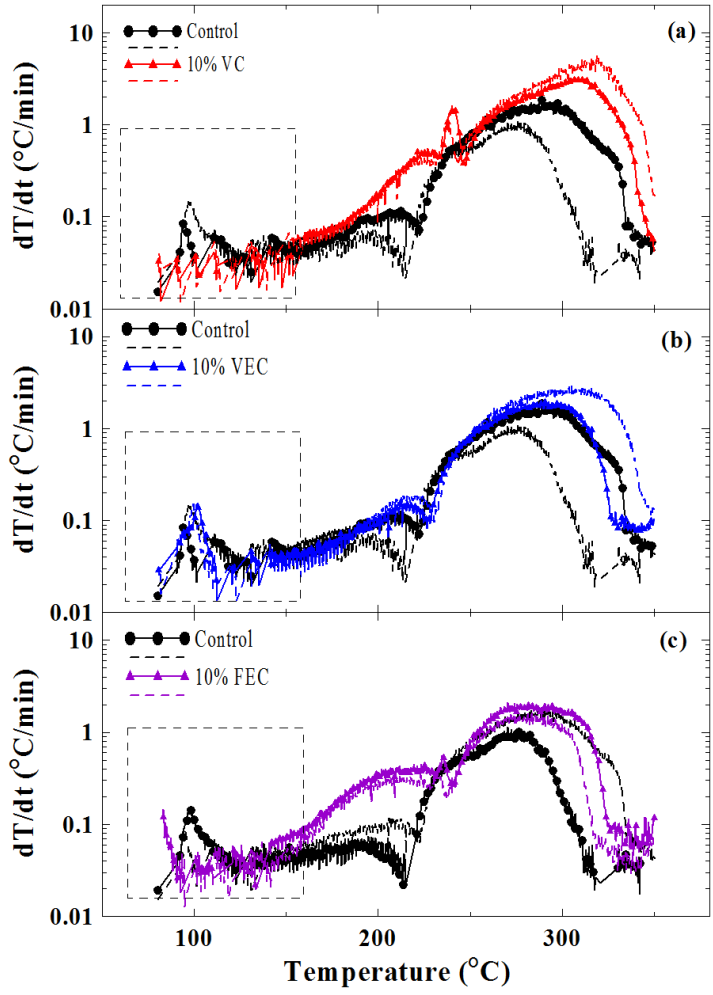

Figure 4.4 Self-heating rate vs. temperature for lithiated graphite reacting with 1M $LiPF_6$ in EC/DEC with 10 wt% VC (a), with 10 wt% VEC (b) or with 10 wt% FEC (c) compared with the control electrolyte.

Since 10 wt% VC and 10 wt% FEC showed some differences in self-heating rate versus temperature compared to the control electrolyte, it is useful to examine any effect that may occur as the concentration of these additives is changed. In order to increase the sensitivity of the experiments in the low temperature region, the masses of lithiated

graphite and electrolyte were both increased to 140 mg for the experiments reported next. Figure 4.5 shows SHR versus temperature results for 140 mg lithiated graphite heated with 140 mg 1M $LiPF_6$ in EC/DEC with 2 wt%, 5 wt% and 10 wt% VC compared with control electrolyte between 50°C and 350°C. The results with 2 wt% VC show that the exothermic peak around 100°C still appeared but its SHR was lower than that of control. Furthermore, there was no obvious exothermic peak around 100°C that could be distinguished when the concentration of VC reached 5 or 10 wt%, which indicates the formation of a more robust SEI. However, as the VC concentration increased, the SHR increased above 130°C. Figure 4.5 shows that VC with various concentrations could help decrease the thermal reactivity of lithiated graphite and the electrolyte below 130°C, especially higher concentrations of VC. Above 130°C, lower concentrations of VC are better for decreasing the intensity of exothermic reactions.

Figure 4.6 shows the SHR versus temperature results for 140 mg lithiated graphite heated with 140 mg 1M $LiPF_6$ in EC/DEC with 2 wt%, 5 wt% and 10 wt% FEC compared with control electrolyte between 50°C and 350°C. The starting temperature was decreased to 50°C mainly in order to see the influence of FEC on the onset temperature of the reactions. The results show that when FEC at 5 or 10% concentration was used, the onset temperature for reaction was 50°C, much lower than that of the control electrolyte. Furthermore, with the increase of FEC concentration, the SHR above 130°C became higher and higher. However, FEC can help eliminate the exothermic peak around 100°C resulting from the decomposition of metastable SEI which forms in the

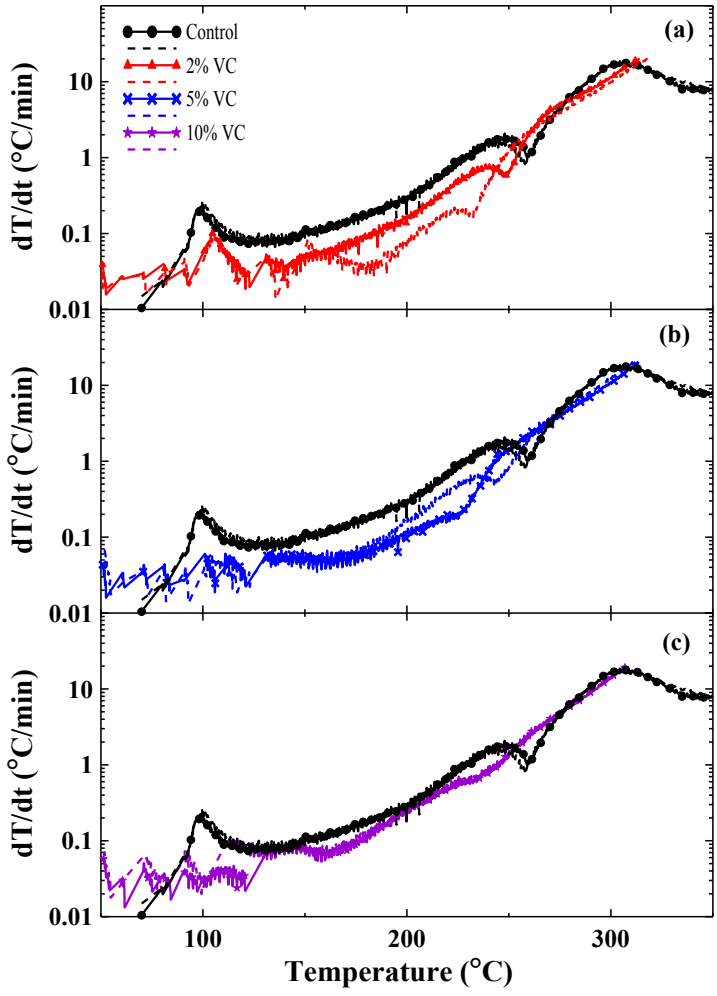

Figure 4.5 Self-heating rate vs. temperature for lithiated graphite reacting with 1M $LiPF_6$ in EC/DEC with 2 wt%, 5 wt% and 10 wt% VC compared with the control electrolyte.

control electrolyte. Electrolytes using large concentrations of FEC (much more than 10% FEC) have been proposed for Li-ion cells containing alloy negative electrodes[80] and also for Li-ion cells proposed for high voltage operation.[81] Given that reactions between the charged negative electrode and FEC-containing electrolyte begin as low as 50°C (Figure 4.6, 5% and 10% FEC) one wonders about the high temperature operation of such cells.

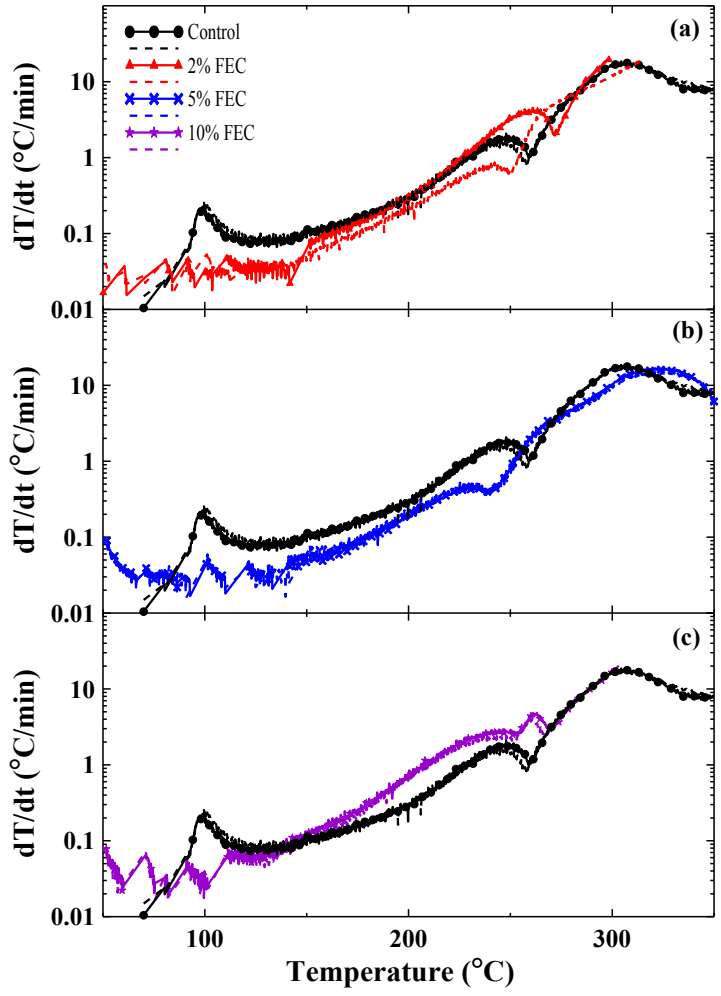

Figure 4.6 Self-heating rate vs. temperature for lithiated graphite reacting with 1M $LiPF_6$ in EC/DEC with 2 wt%, 5 wt% and 10 wt% FEC compared with the control electrolyte.

4.1.3 CONCLUSION

The effects of the electrolyte additives, VC, VEC and FEC on the reactivity of delithiated NMC or lithiated graphite with electrolyte were studied using ARC. The results can be summarized as follows:

(1) VC, FEC and VEC have no obvious effect on the reactivity of delithiated NMC with electrolyte at elevated temperatures.

(2) 10 wt% VEC does not have an impact on the reactivity of lithiated graphite with electrolyte. VEC seems benign as an electrolyte additive from a safety perspective.

(3) VC can help increase the thermal stability of the lithiated graphite and deserves further study, especially in combinations with other electrolyte additives that allow high concentrations of VC to be considered, in light of the increase in impedance that high VC concentrations, alone, causes.[82]

(4) High concentrations of FEC lead to a low temperature exotherm (50°C) between lithiated graphite and electrolyte. This suggests the elevated temperatures performance of cells with large amounts of FEC may be affected. In addition, when high concentrations of FEC are used (10%), the reactivity between lithiated graphite and electrolyte increases (compared to control electrolyte) at temperatures above 130°C.

(5) Use of the electrolyte additives VC and FEC at the 2 wt% level has very little impact on the reactivity between electrolyte and charged electrode materials at elevated temperatures. However, apart from VEC, higher concentrations do impact reactivity as mentioned above.

4.2 COMPARISON OF THE EFFECT OF VARIOUS SULFUR-CONTAINING AND PHOSPHORUS-CONTAINING

ADDITIVES ON THE REACTION BETWEEN CHARGED ELECTRODES AND ELECTROLYTES

4.2.1 EXPERIMENTAL

NMC111 and graphite (MCMB) were chosen as the materials for this study. These were the same materials described in section 4.1. Charged electrode materials and electrolyte containing 2 wt% of various additives were put in the ARC tubes for the tests. The additives selected were ethylene sulfate (DTD, Sigma-Aldrich, 98%), 1,3-propanediol cyclic sulfate (TMS, Sigma-Aldrich, 99%), propylene sulfate (PLS, Sigma-Aldrich, 99%), methylene methanedisulfonate (MMDS, Tinci Materials Technology, 98.7%), tris(trimethylsilyl) phosphate (TTSP, Sigma-Aldrich, > 98%), tris(trimethylsilyl) phosphite (TTSPi, Sigma-Aldrich, > 95%), prop-1-ene-1,3-sultone (PES, Lianchuang pharmaceutical, 98.2%). Figure 4.7 shows the chemical structures of the additives studied in this section.

During the ARC test, the starting temperature was set to be 70°C or 50°C for positive or negative electrode tests, respectively. ARC tests were tracked under adiabatic conditions when the sample SHR exceeded 0.03°C/min. Experiments were stopped at 350°C or when the SHR exceeded 20°C/min.

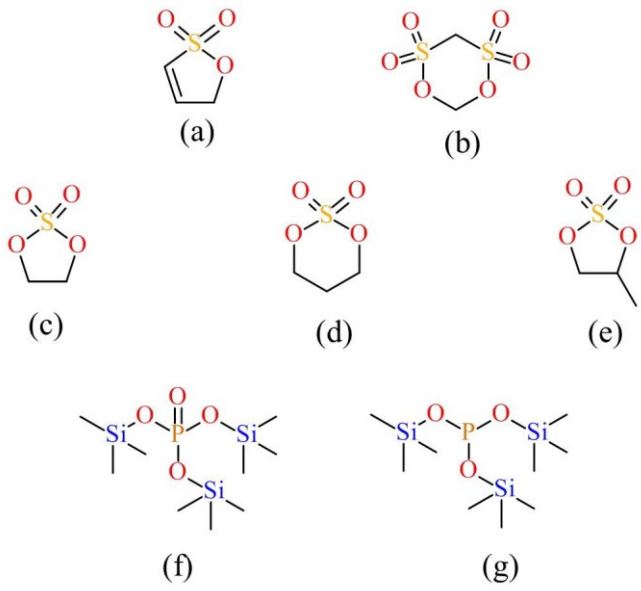

Figure 4.7 Chemical structures of the electrolyte additives used (a) prop-1-ene-1,3-sultone (PES) (b) methylene methanedisulfonate (MMDS) (c) ethylene sulfate (DTD) (d) 1,3-propylene sulfate (TMS) (e) propylene sulfate (PLS) (f) tris(trimethylsilyl) phosphate (TTSP) and (g) tris(trimethylsilyl) phosphite (TTSPi).

4.2.2 RESULTS AND DISCUSSION

Figure 4.8 shows the results of ARC experiments on 94 mg delithiated NMC reacting with 30 mg electrolyte containing 2 wt% MMDS (a) and 140 mg lithiated graphite reacting with 140 mg electrolyte containing 2 wt% MMDS (b) compared with the results for the control electrolyte. Each experiment was repeated and Figures 4.8(a) and (b) show that the results were highly reproducible. Figure 4.8(a) shows that 2 wt% MMDS yielded a significant improvement in thermal stability compared to control by decreasing the SHR after 250°C. The most striking feature of Figure 4.8(b) is that 2% MMDS

showed no exothermic feature at around 100°C thought to be caused by the decomposition of the metastable SEI on the lithiated graphite, which suggests a very

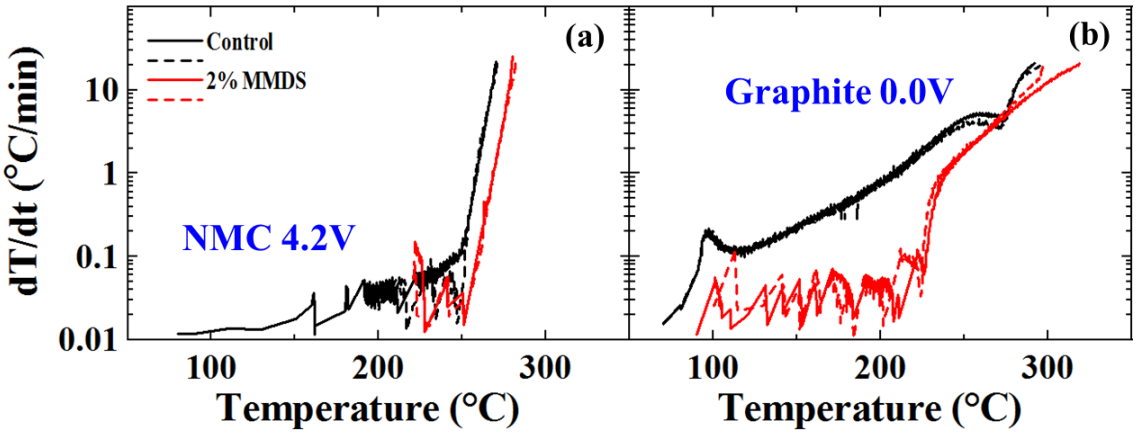

Figure 4.8 Self-heating rate vs. temperature for delithiated NMC (a) or lithiated graphite (b) reacting with 1M $LiPF_6$ in EC/EMC (3/7 wt%) with 2 wt% MMDS compared with the control electrolyte.

thermally stable SEI on the graphite side in the case of 2% MMDS. Furthermore, the SHR versus temperature for 2% MMDS was lower than that of the control sample over the entire testing range. The ARC results in Figure 4.8 show that MMDS reduced the reactivity between charged electrode materials and electrolyte and the use of MMDS could lead to safer Li-ion cells.

Figure 4.9 shows the results of ARC experiments on 94 mg delithiated NMC reacting with 30 mg electrolyte containing 2 wt% PES (a) and 140 mg lithiated graphite reacting with 140 mg electrolyte containing 2 wt% PES (b) compared with the results for control electrolyte. Figure 4.9(a) shows that 2% PES reduced the reactivity of delithiated NMC

and electrolyte above 250°C. The results for the graphite electrode in Figure 4.9(b) show that when 2% PES was used, the onset temperature for a small exothermic reaction was 50°C which is much lower than that of the control electrolyte. In addition, 2% PES resulted in a higher SHR between ~ 100°C and ~ 150°C compared to control electrolyte

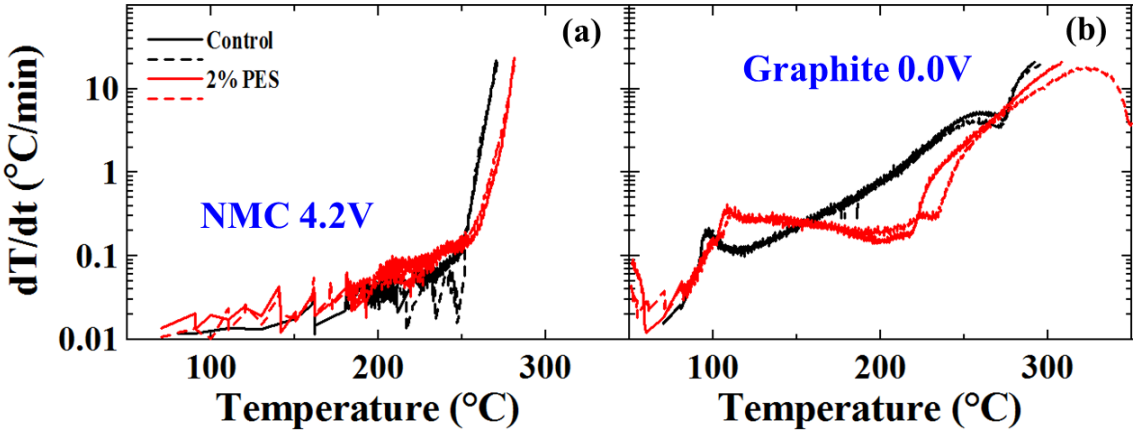

Figure 4.9 Self-heating rate vs. temperature for delithiated NMC (a) or lithiated graphite (b) reacting with 1M $LiPF_6$ in EC/EMC (3/7 wt%) with 2 wt% PES compared with the control electrolyte.

but 2% PES also decreased the self-heating rate between ~ 150°C and ~ 260°C compared to control electrolyte.

Figure 4.10 shows the results of ARC experiments on 94 mg delithiated NMC reacting with 30 mg electrolyte containing 2 wt% DTD (a) and 140 mg lithiated graphite reacting with 140 mg electrolyte containing 2 wt% DTD (b) compared with the results for control electrolyte. In Figure 4.10(a), 2% DTD and control electrolyte had virtually the same response for the reaction between delithaited NMC and electrolyte. For the graphite

electrode, with the addition of 2% DTD, the SHR versus temperature was a little lower than that of the control sample over almost the entire testing range.

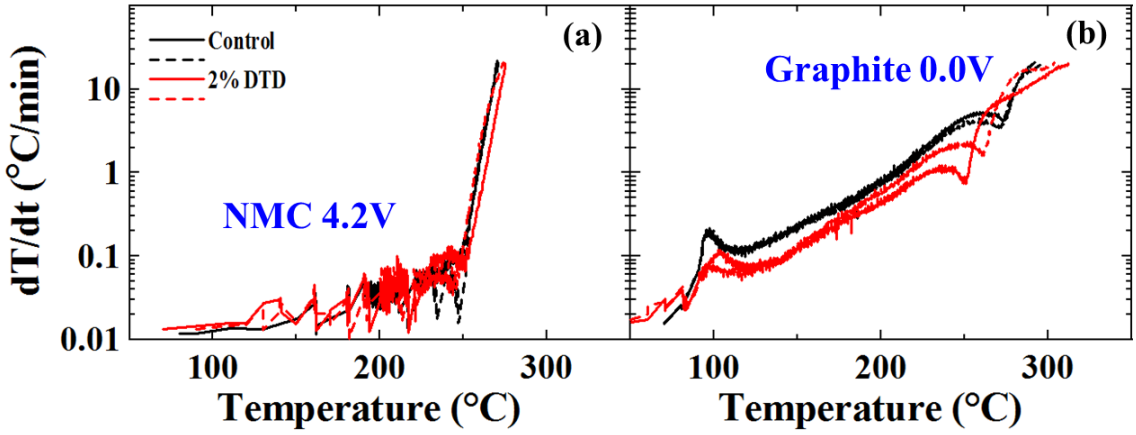

Figure 4.10 Self-heating rate vs. temperature for delithiated NMC (a) or lithiated graphite (b) reacting with 1M $LiPF_6$ in EC/EMC (3/7 wt%) with 2 wt% DTD compared with the control electrolyte.

Figure 4.11 shows the results of ARC experiments on 94 mg delithiated NMC reacting with 30 mg electrolyte containing 2 wt% TMS (a) and 140 mg lithiated graphite reacting with 140 mg electrolyte containing 2 wt% TMS (b) compared to the results for control electrolyte. In Figure 4.11(a), there is almost no difference between the sample with 2% TMS and control sample. In Figure 4.11(b), an exothermic reaction was detected at around 75°C with the addition of 2% TMS for the lithiated graphite sample, which is lower than the onset temperature of control electrolyte (~ 85°C). In addition, after around 90°C, 2% TMS yielded a slightly lower self-heating rate up to 350°C compared to control electrolyte.

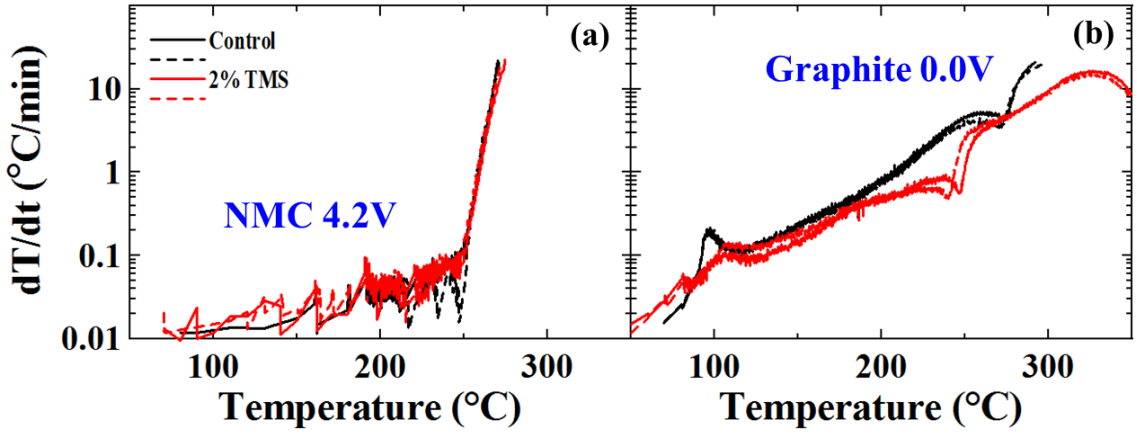

Figure 4.11 Self-heating rate vs. temperature for delithiated NMC (a) or lithiated graphite (b) reacting with 1M $LiPF_6$ in EC/EMC (3/7 wt%) with 2 wt% TMS compared with the control electrolyte.

Figure 4.12 shows the results of ARC experiments on 94 mg delithiated NMC reacting with 30 mg electrolyte containing 2 wt% PLS (a) and 140 mg lithiated graphite reacting with 140 mg electrolyte containing 2 wt% PLS (b) compared to the results for control electrolyte. Figure 4.12(a) shows that 2% PLS did not have a strong impact on the reaction between delithiated NMC and electrolyte. Figure 4.12(b) shows that the reaction between lithiated graphite and electrolyte was also very similar to that of control electrolyte. The only effect of 2% PLS can be seen in Figure 4.12(b) where the self-heating rate was decreased in the temperature range from ~ 150°C to ~ 250°C.

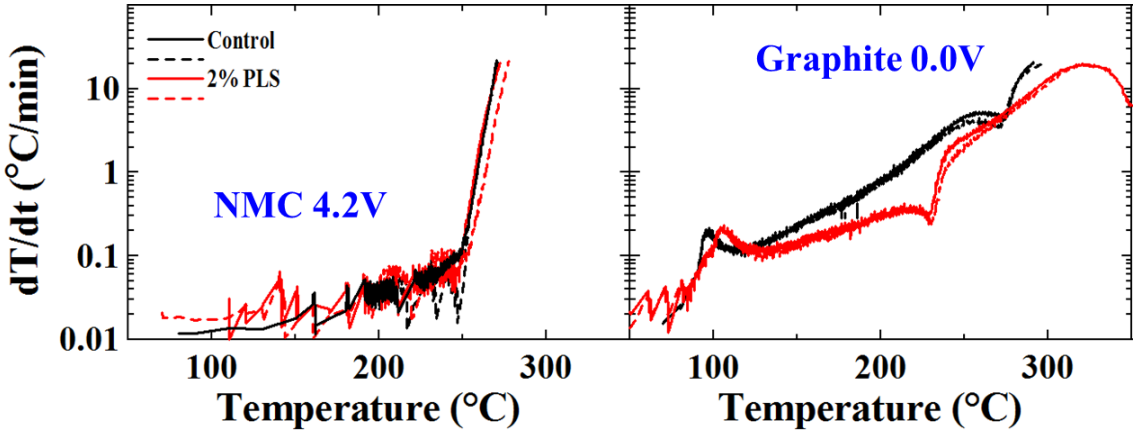

Figure 4.12 Self-heating rate vs. temperature for delithiated NMC (a) or lithiated graphite (b) reacting with 1M $LiPF_6$ in EC/EMC (3/7 wt%) with 2 wt% PLS compared with the control electrolyte.

Figure 4.13 shows the results of ARC experiments on 94 mg delithiated NMC reacting with 30 mg electrolyte containing 2 wt% TTSPi (a) and 140 mg lithiated graphite reacting with 140 mg electrolyte containing 2 wt% TTSPi (b) compared to the results for control electrolyte. Figure 4.13(a) shows that the addition of 2% TTSPi helps suppress the rapid exothermic reaction between delithiated NMC and electrolyte after 250°C and the thermal runaway temperature also increases by ~ 10°C compared to the control electrolyte. Additionally, Figure 4.13 shows that the self-heating rate between ~ 150°C and ~ 200°C was reduced with the addition of 2% TTSPi for the reaction between lithiated graphite and electrolyte.

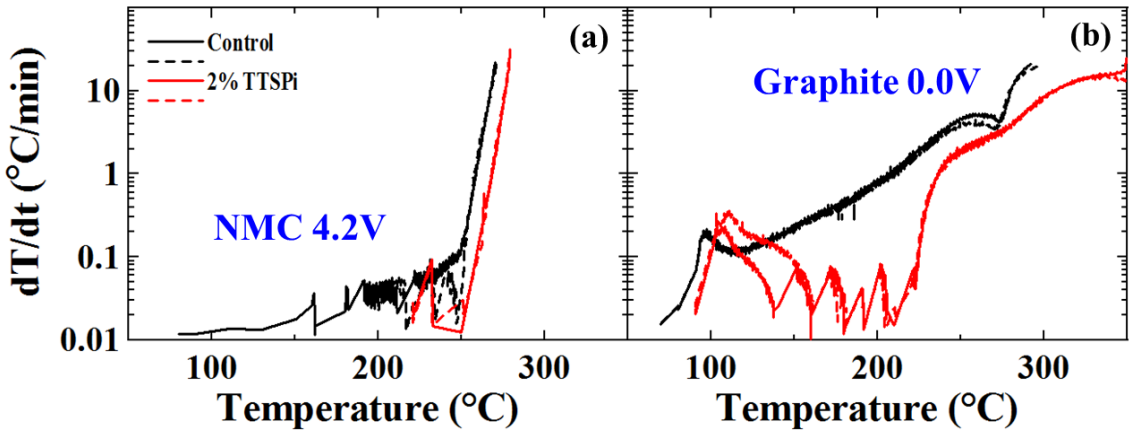

Figure 4.13 Self-heating rate vs. temperature for delithiated NMC (a) or lithiated graphite (b) reacting with 1M $LiPF_6$ in EC/EMC (3/7 wt%) with 2 wt% TTSPi compared with the control electrolyte.

Figure 4.14 shows the results of ARC experiments on 94 mg delithiated NMC reacting with 30 mg electrolyte containing 2 wt% TTSP (a) and 140 mg lithiated graphite reacting with 140 mg electrolyte containing 2 wt% TTSP (b) compared to the results for control electrolyte. The effect of 2% TTSP on the reaction between charged electrodes and electrolyte was not dramatic according to the results shown in Figures 4.14(a) and (b). However, 2% TTSP decreased the self-heating rate at around 100°C caused by the decomposition of the metastable SEI for the lithiated graphite electrode.

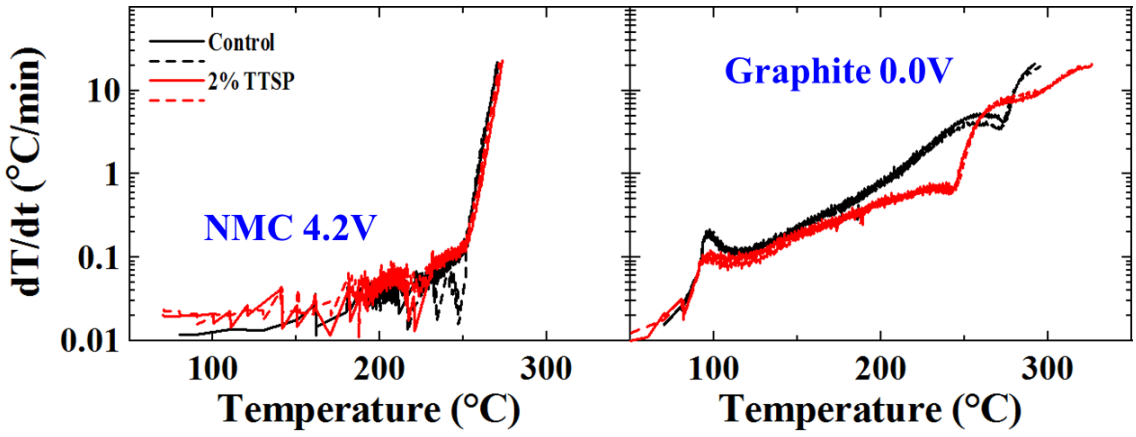

Figure 4.14 Self-heating rate vs. temperature for delithiated NMC (a) or lithiated graphite (b) reacting with 1M $LiPF_6$ in EC/EMC (3/7 wt%) with 2 wt% TTSP compared with the control electrolyte.

4.2.3 CONCLUSION

The effect of various sulfur-containing (PES, MMDS, DTD, TMS, PLS) and phosphorus-containing (TTSPi, TTSP) additives on the reaction between charged electrodes (delithiated NMC or lithiated graphite) and electrolytes was studied using ARC in this work. All the additives used in this work were at the level of 2 wt%.

Most of the selected additives do not have a dramatic effect on the reaction between delithiated NMC and electrolyte compared to control sample, except for PES, MMDS and TTSPi. These three additives at the level of 2 wt% decreased the self-heating rate after ~ 250°C.

Unlike delithiated NMC, the reactivity between lithiated graphite and electrolyte was affected more or less by all the additives used in this work. The most interesting are the

effects of MMDS and TTSPi at the level of 2 wt%: MMDS helped suppress obvious exothermic reactions up to ~ 200°C while TTSPi dramatically decreased self-heating rates in the temperature range between ~ 150°C and ~ 200°C. In case of DTD, TMS and TTSP, the self-heating rate decreased slightly during almost the entire test temperature range. It is unfortunate that 2 wt% PES did not give a beneficial effect on the reaction between lithiated graphite and electrolyte. In addition, when PES was used, there was a small exothermic reaction with an onset temperature of 50°C which the control electrolyte did not show.

Based on the effects observed in experiments of charged positive and negative electrodes, it is believed that the heat produced during abuse scenarios involving lithium-ion cells can be reduced using MMDS or TTSPi.

4.3 EXPLORATION OF THE EFFECT OF SOME PROMISING ADDITIVE COMBINATIONS ON THE REACTION BETWEEN CHARGED ELECTRODES AND ELECTROLYTES USING ACCELERATING RATE CALORIMETRY

4.3.1 EXPERIMENTAL

NMC111 and graphite (MCMB) were chosen as the materials for this study. These were the same materials described in section 4.1. Charged electrode materials and electrolyte containing selected additive combinations were put in the ARC tubes for the tests.

During the ARC test, the starting temperature was set to be 70°C or 50°C for positive or negative electrode tests, respectively. ARC tests were tracked under adiabatic conditions when the sample SHR exceeded 0.03°C/min. Experiments were stopped at 350°C or when the SHR exceeded 20°C/min. In order to demonstrate the advantages of these promising additive combinations, some long-term cycling results are shown in this section and compared to results for control electrolyte or for electrolyte with only one additive. All the NMC111/graphite pouch cells were cycled between 2.8 V and 4.2 V with a current of 80 mA (C/2.5) at 55°C. Gas production during long-term cycling was measured using Archimedes' principle with cells suspended from a balance while submerged in a beaker of de-ionized "nanopure" water at 20. ± 1°C.[83] The process of fabricating pouch cells can be found in the Master's thesis (2014) of K. J. Nelson.[84] The long-term cycling work here was done in collaboration with Jian Xia (a visiting Ph.D student).

4.3.2 RESULTS AND DISCUSSION

Some promising VC-based and PES-based additive combinations were selected to be evaluated during long-term cycle testing at 55°C between 2.8 V and 4.2 V with a current of 80 mA. Since the pouch cells used for this test were unclamped, any gas production during cycling could result in the reduction of stack pressure in the cells. Figure 4.15 shows capacity versus cycle number for NMC111/graphite pouch cells (unclamped) with the VC-based additive blends: 2% VC, 3% VC, 2% VC + 1% DTD, 2% VC + 2% TMS, 2% VC + 1% MMDS and 2% VC + 1% MMDS + 1% TTSPi. The ternary blends show

the best capacity retention compared to all the binary blends and VC alone. All the selected binary blends are better than both 2% VC and 3% VC until 500 cycles, which indicates that simply adding more VC is not as effective as combining VC with other additives.

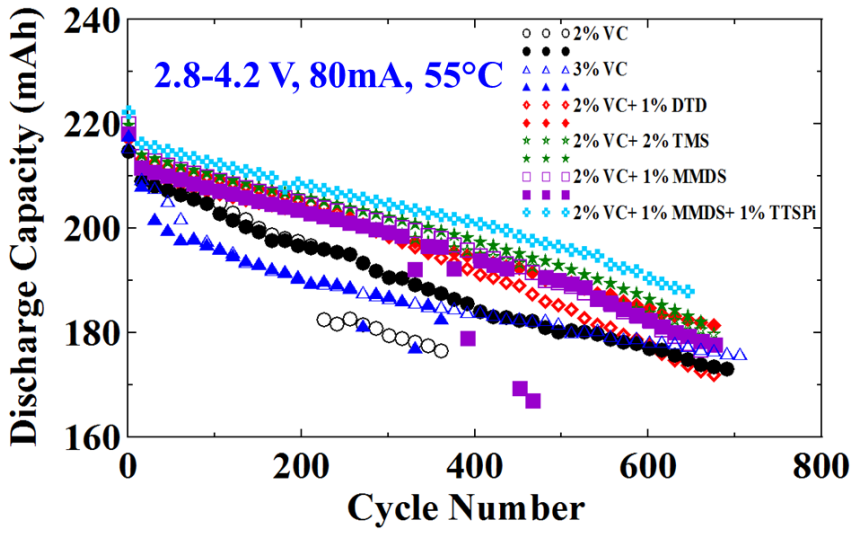

Figure 4.15 Capacity versus cycle number for NMC111/graphite pouch cells (unclamped) containing the indicated VC-based binary or ternary additive blends. The cycling was done between 2.8 and 4.2 V at 55°C and at 80 mA.

Figure 4.16 shows the amount of gas evolved for VC-based additives during the long-term cycling period. All the VC-based combinations produced less gas than VC itself during the long-term cycling process, especially 2% VC + 1% MMDS + 1% TTSPi with ~ 0.1 mL gas even after 500 cycles. This showed the advantage of additive blends in suppressing gas production during cycling.

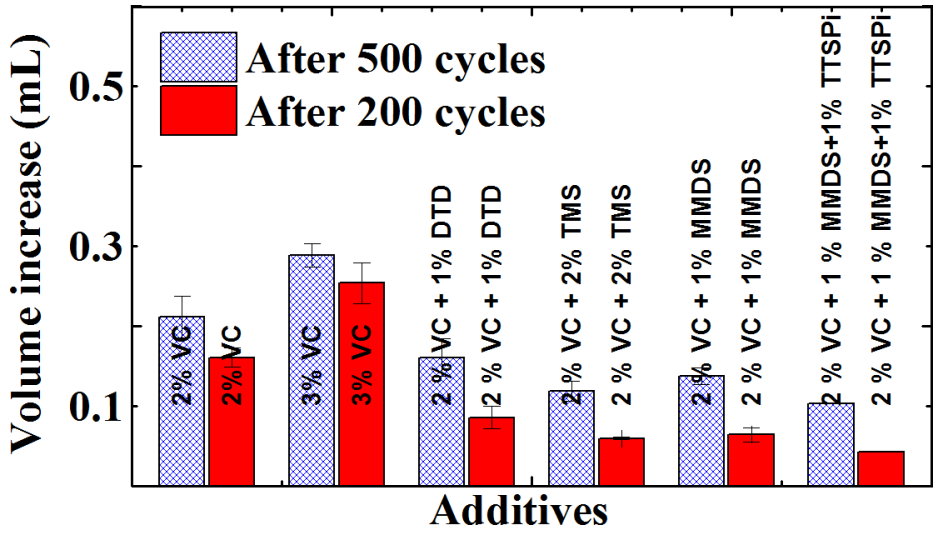

Figure 4.16 Volume of gas evolved during long-term cycling for the NMC111/graphite pouch cells (unclamped) containing the indicated VC-based binary or ternary additive blends. The cycling was done between 2.8 and 4.2 V at 55°C and at 80 mA. Each bar represents the average of data collected for 2 cells and the error bars represent the standard deviation of the data.

Figure 4.17 shows capacity versus cycle number for NMC111/graphite pouch cells (unclamped) with the PES-based additive blends: 2% PES, 3% PES, 2% PES + 1% MMDS + 1% TTSPi. Again, the selected ternary additive blend shows much better capacity retention than PES itself, which suggests the advantage of combinations with other additives.

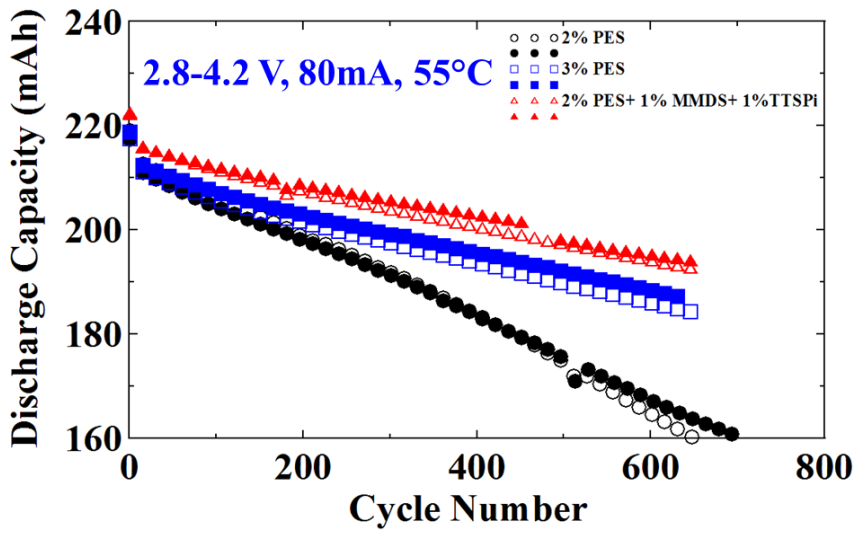

Figure 4.17 Capacity versus cycle number for NMC111/graphite pouch cells (unclamped) containing the indicated PES-based ternary additive blends. The cycling was done between 2.8 and 4.2 V at 55°C and at 80 mA.

Figure 4.18 shows the increase of cell volume for NMC111/graphite pouch cells with PES-based additives during the long-term cycling period. The volume increase of the cells containing PES-based additive blends or 3% PES was very small, which suggests good stack pressure during long-term cycling. Considering that PES can dramatically suppress gas production during formation and cycling,[85] the small expansion of the cells may be caused by electrode thickness expansion, not gas production, which needs to be investigated in detail in future.

Based on the results shown above, the advantages of selected additive blends in capacity retention and suppression of gas production is obvious. Therefore it is important to

evaluate their effect on the reactions between charged electrodes and electrolytes to be sure their adoption would not lead to safety concerns.

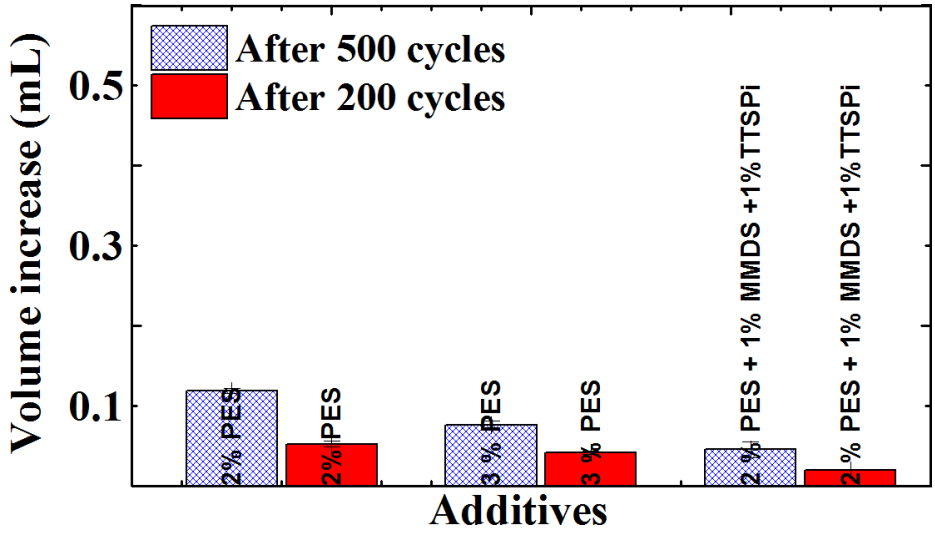

Figure 4.18 The cell volume increase after long time cycling for the NMC111/graphite pouch cells (unclamped) containing the indicated PES-based ternary additive blends. The cycling was done between 2.8 and 4.2 V at 55°C and at 80 mA. Each bar represents the average of data collected for 2 cells and the error bars represent the standard deviation of the data.

Figure 4.19 shows the results of ARC experiments on 140 mg lithiated graphite reacting with 140 mg electrolyte containing 2 wt% VC + 2 wt% MMDS compared to the results for control electrolyte. With the addition of 2% VC + 2% MMDS, there was almost no obvious exothermic reaction that could be detected up to ~ 150°C but the self-heating rate became higher than that of control after ~ 230°C.

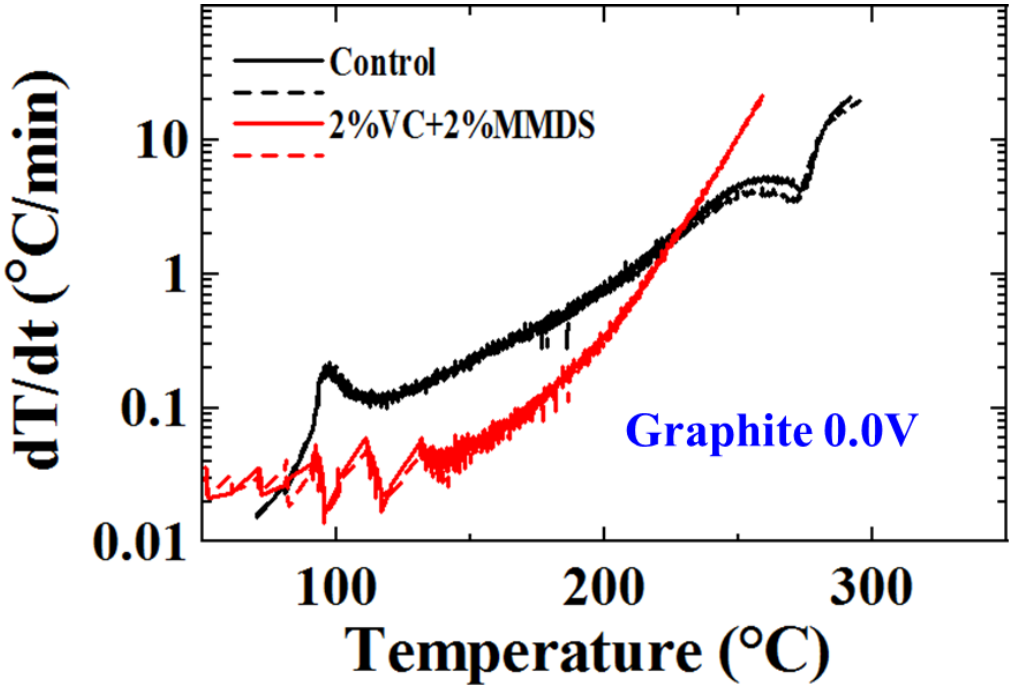

Figure 4.19 Self-heating rate vs. temperature for lithiated graphite reacting with 1M $LiPF_6$ in EC/EMC (3/7 wt%) with 2 wt% VC + 2 wt% MMDS compared with the control electrolyte.

Figure 4.20 shows the results of ARC experiments on 140 mg lithiated graphite reacting with 140 mg electrolyte containing 2 wt% VC + 2 wt% DTD compared to the results for control electrolyte. With the addition of 2% VC + 2% DTD, the self-heating rate became lower than that of control over the entire temperature range. However, a tiny exothermic reaction could be detected near 50°C.

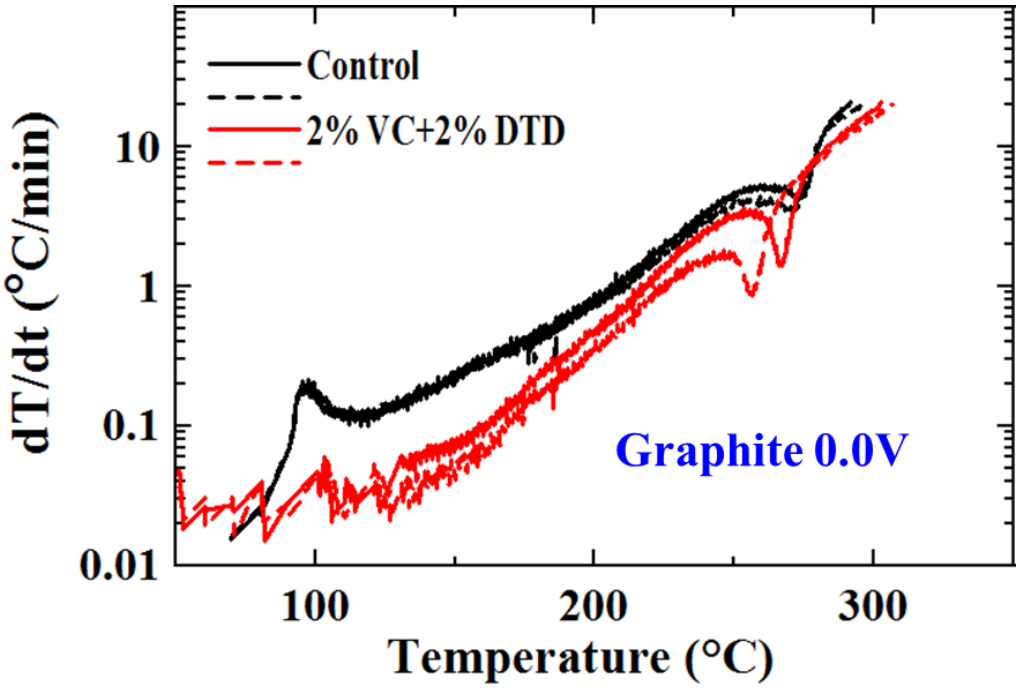

Figure 4.20 Self-heating rate vs. temperature for lithiated graphite reacting with 1M $LiPF_6$ in EC/EMC (3/7 wt%) with 2 wt% VC + 2 wt% DTD compared with the control electrolyte.

Figure 4.21 shows the results of ARC experiments on 94 mg delithiated NMC reacting with 30 mg electrolyte containing 2 wt% VC + 2 wt% TMS (a) and 140 mg lithiated graphite reacting with 140 mg electrolyte containing 2 wt% VC + 2 wt% TMS (b) compared to the results of control electrolyte. Figure 4.21(a) shows that the addition of 2 wt% VC + 2 wt% TMS suppressed the rapid exothermic reaction between delithiated NMC and electrolyte after 250°C. However, this additive combination was not helpful in the temperature range between ~ 200°C and ~ 250°C. Figure 4.21(b) shows that 2 wt%

VC + 2 wt% TMS decreased the self-heating rate almost over the entire temperature range for the reaction between lithiated graphite and electrolyte except for a tiny exothermic reaction near 50°C.

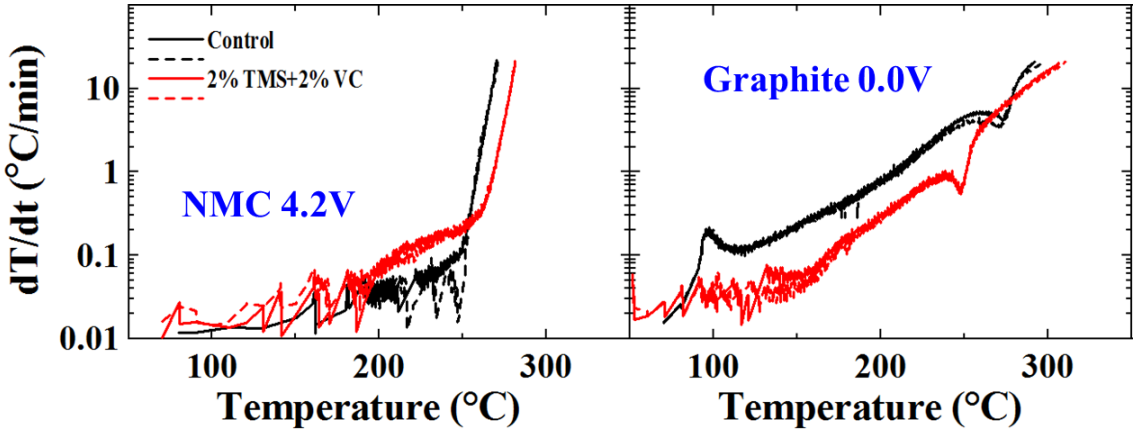

Figure 4.21 Self-heating rate vs. temperature for delithiated NMC (a) or lithiated graphite (b) reacting with 1M $LiPF_6$ in EC/EMC (3/7 wt%) with 2 wt% VC + 2 wt% TMS compared with the control electrolyte.

Figure 4.22 shows the results of ARC experiments on 140 mg lithiated graphite reacting with 140 mg electrolyte containing 2 wt% VC + 1 wt% MMDS + 1 wt% TTSPi compared with the results for the control electrolyte. This VC-based "211" blend shows no exothermic feature at around 100°C thought to result from the decomposition of the metastable components of the SEI on the lithiated graphite, which indicates a very robust SEI. In addition, the self-heating-rate versus temperature was lower than that of the control sample over the entire testing range.

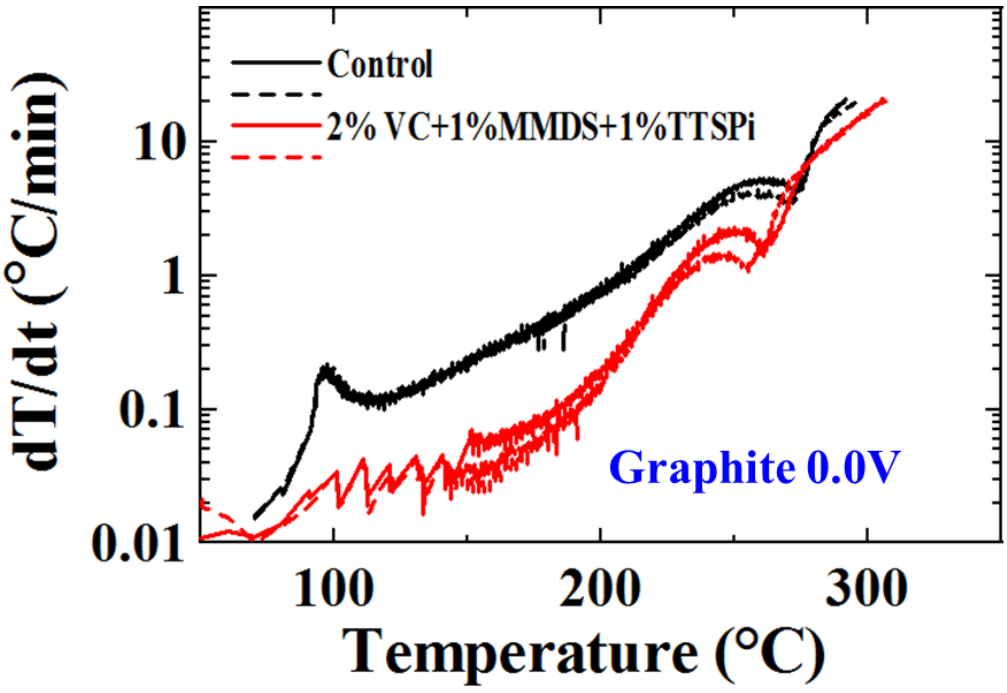

Figure 4.22 Self-heating rate vs. temperature for lithiated graphite reacting with 1M $LiPF_6$ in EC/EMC (3/7 wt%) with 2 wt% VC + 1 wt% MMDS + 1 wt% TTSPi compared with the control electrolyte.

Figure 4.23 shows the results of ARC experiments on 140 mg lithiated graphite reacting with 140 mg electrolyte containing 2 wt% PES + 1 wt% MMDS + 1 wt% TTSPi compared with the results for the control electrolyte. Again, this PES-based "211" blend dramatically decreased the exothermic feature at around 100°C thought to be caused by the decomposition of the metastable components of the SEI on the lithiated graphite. Additionally, the self-heating-rate versus temperature is lower than that of the control sample over almost the entire testing range.

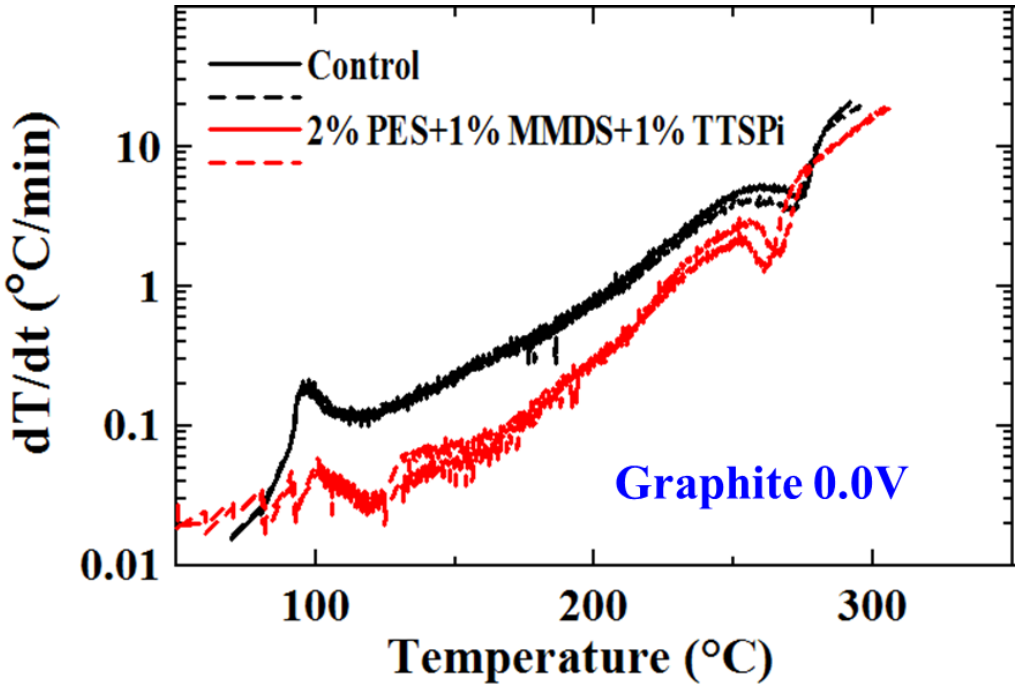

Figure 4.23 Self-heating rate vs. temperature for lithiated graphite reacting with 1M $LiPF_6$ in EC/EMC (3/7 wt%) with 2 wt% PES + 1 wt% MMDS + 1 wt% TTSPi compared with the control electrolyte.

As a note in passing, it was not possible to measure the self-heating rate versus temperature for the 2% VC + 2% MMDS, 2% VC + 2% DTD, 2% VC + 1% MMDS + 1% TTSPi and 2% PES + 1% MMDS + 1% TTSPi blends reacting with delithiated NMC due to corrosion of the thin walled stainless steel ARC tube at the welded ends at elevated temperatures (> 200°C). However, this feature of these blends will not be problematic in pouch cells which contain no ferrous metals.

4.3.3 CONCLUSION

Compared to cells with VC or PES alone, cells with selected additive combinations such as 2%VC + 1%MMDS + 1%TTSPi, 2%PES + 1%MMDS + 1%TTSPi etc. gave better capacity retention and smaller amounts of gas generation during long-term cycling at 55°C. All the selected additive combinations decreased the self-heating rate of reactions between lithiated graphite and electrolyte compared to control electrolyte, which suggests a more thermally stable SEI on the negative electrode.

It is clear that some additive combinations can bring significant benefits to NMC111/graphite cells by leading to longer life time and better safety.

A patent[86] was filed based on the work described in this thesis and based on other work done in the Dahn group.

CHAPTER 5. CONCLUSIONS AND FUTURE WORK

5.1 CONCLUSIONS

A method using ARC has been developed to study the effects of selected additives or combinations of additives on the reactions between charged electrode materials and electrolytes at elevated temperatures. NMC111 and graphite (MCMB) were used as the positive electrode material and the negative electrode material, respectively, for the studies in this thesis.

The effects of some traditional additives (VC, FEC and VEC) were evaluated using ARC. VC, FEC and VEC did not have a major effect on the reactivity of delithiated NMC with electrolyte. VEC did not affect the reactivity of lithiated graphite with electrolyte either at the levels up to 10 wt%. Both VC and FEC (2, 5 or 10 wt%) decreased the exothermic peak at around 100°C caused by the decomposition of the metastable SEI on lithiated graphite. However, high concentrations of FEC (5 or 10 wt%) caused a lower onset temperature (50°C) compared to control electrolyte.

Except for the traditional electrolyte additives, the effects of some novel sulfur-containing and phosphorus-containing additives on the reactivity between charged electrodes and electrolytes at elevated temperatures were also studied using ARC. Generally, most of the selected additives (DTD, TMS, PLS and TTSP) did not strongly affect the reactivity of delithiated NMC with electrolyte except for PES, MMDS and TTSPi which decreased the self-heating rate after ~ 250°C. For the reactivity of lithiated graphite with electrolyte, MMDS and TTSPi dramatically decreased the self-heating rate.

There was barely an exothermic reaction till ~ 200°C with addition of 2% MMDS. 2% TTSPi strongly decreased the self-heating rate between ~ 150°C and ~ 200°C. Unfortunately, 2% PES used alone lead to a lower onset temperature (~ 50°C) compared to control electrolyte.

Some promising additive combinations showed their advantages compared to 2% PES or 2% VC used alone during long-term cycling tests. These selected additive combinations yielded good capacity retention and tiny gas production after 600 cycles at 55°C. Some cells retained 90% of their initial capacity after 600 cycles, which is excellent performance. The influence of these additive combinations on the reactivity between charged electrodes and electrolytes was measured using ARC. Selected ternary additive combinations such as 2% VC + 1% MMDS + 1% TTSPi and 2% PES + 1% MMDS + 1% TTSPi dramatically decreased the self-heating rate between lithiated graphite and electrolyte over the entire temperature range, which suggests a thermally stable SEI on the negative electrode.

The electrolyte combination “2% PES + 1% MMDS + 1% TTSPi” is the best known for NMC111/graphite cells operating to 4.2 V. It has been given the name “Lin Special” in our laboratory.

5.2 FUTURE WORK

5.2.1 STUDY OF GASEOUS PRODUCTS AFTER ARC TESTING

Figure 5.1 shows the ARC tube before (a) and after (b) testing at elevated temperatures, respectively. The stainless steel tube becomes swelled after testing in the ARC because of the production of some unknown gas. The gaseous by-products can give a clue about

Figure 5.1 Stainless steel tube before ARC testing (a) and after ARC testing (b).

the exothermic reactions which happened during the test at elevated temperatures. However, there is no previous experience in our lab about the gaseous species produced. The use of gas chromatography coupled with mass spectrometry (GC-MS) can identify the gases. Gas chromatography (GC) separates neutral compounds that exist in the gas phase while mass spectrometry (MS) identifies the chemical structure of the compounds. In order to collect the gas product without contamination from air, a container with a punch needle, shown in Figure 5.2, was designed. Figure 5.2(a) shows the designed gas-extraction tool. Some parts labelled with capital letters need to be described here: A is a quick connect for the connection to a vaccum pump or an Ar gas line; B is the port where a gas sample can be extracted with syringe; C is the punch which seals to the lid and is

used to punch open the ARC tube. Figure 5.2(b) shows some parts of the inside of this device clearly. It contains a metal ring and a metal base with a notch to hold the ARC tube.

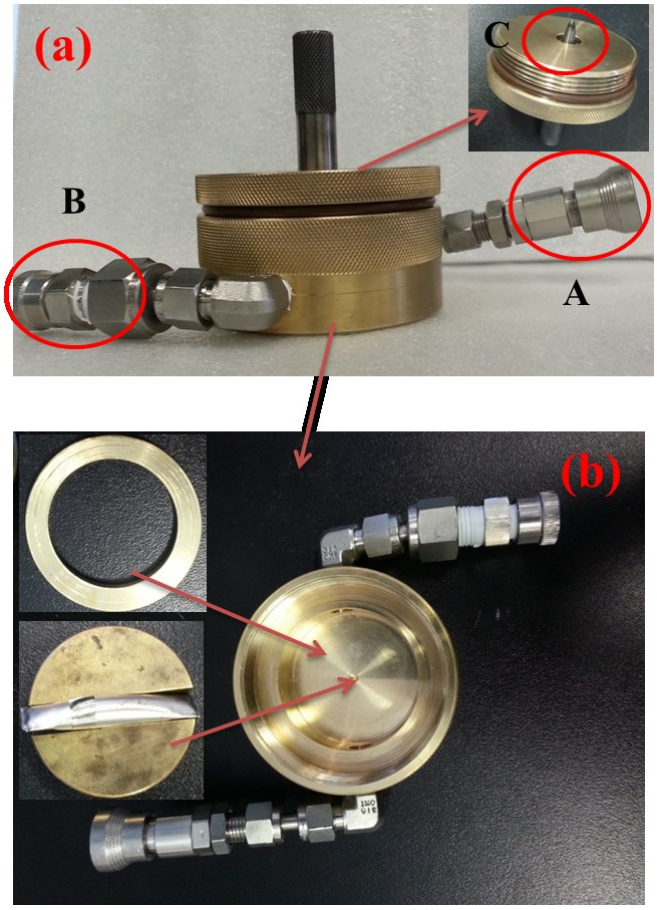

Figure 5.2 A home-made gas-extraction tool for GC-MS testing of gases created during ARC testing (a). Some parts of this container are shown in detail (b).

Before extracting gas from the ARC tube, the device is connected to a vaccum pump to remove air. Then the punch is pushed down to puncture the tube and release the gas inside the device (see Figure 5.3). An Ar gas line is connected to the gas-extraction tool for a few seconds to dilute the gas inside. Finally, a known amount of gas sample (~ 50 μL) can be extracted from this tool using a gas syringe for GC-MS testing.

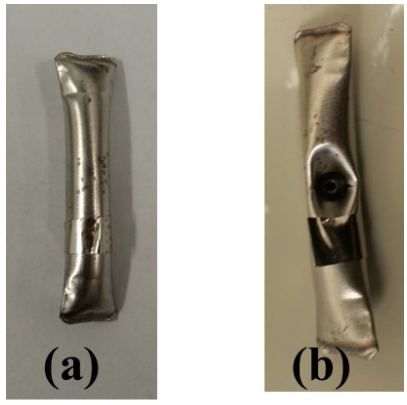

Figure 5.3 The stainless steel tube before punching (a) and after punching (b).

Figure 5.4 shows a chromatogram (total ion counts) of the gas extracted from the tube after ARC testing of 50 mg di-tert-butyl peroxide at elevated temperatures (50 - 350°C). Figure 5.4 shows that the gaseous by-products can be well-separated in a rapid manner. The main gases (labelled in the graph), such as methane, 2-propanone and so on can be clearly identified using GC-MS. Therefore, it is a useful way of testing the gases produced by reactions between charged electrodes and electrolytes at elevated temperatures.

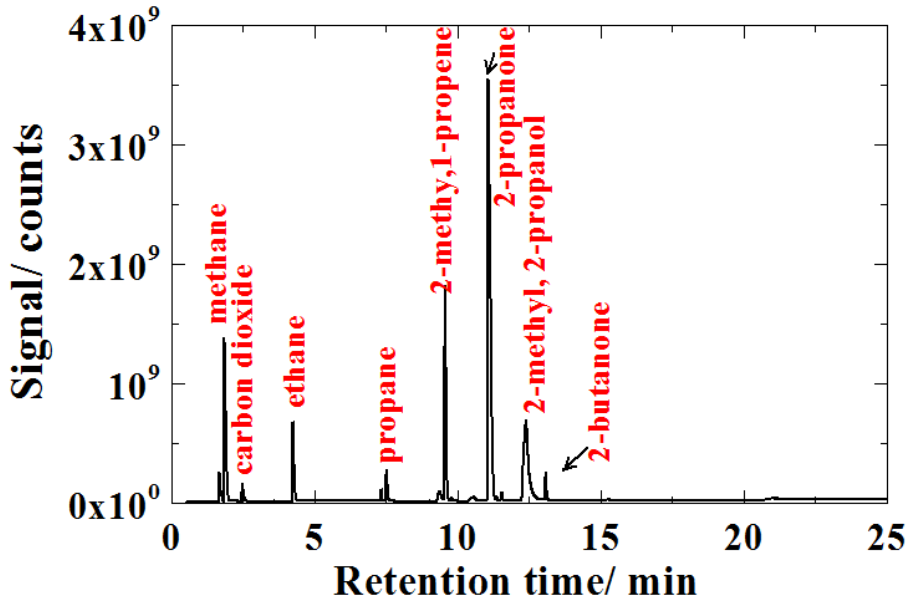

Figure 5.4 Chromatogram (total ion counts) of the gaseous by-products caused by the decomposition of 50 mg DTBP after ARC testing at elevated temperatures (50 - 350°C).

5.2.2 STUDIES OF THE THERMAL STABILITY OF SMALL FULL CELLS AT ELEVATED TEMPERATURES

Richard's and Xia's previous work[11,15] about the reactivity of delithiated positive electrode materials (NMC, LCO etc.) or lithiated negative electrode materials (graphite) with electrolyte was carried out using protocol described in Chapter 2. Thus the thermal performance of the positive side or negative side was measured separately. However, it is also important to study the reactivity of charged electrodes with electrolytes in full cells because this may give more comprehensive information about the exothermic reactions which happen at elevated temperatures. Recently, some small full cells (LCO/LTO, see Figure 5.5) were obtained from Medtronic Company (MN, USA) which are suitable for safety testing using ARC.

Figure 5.5 A 15 mAh small commercial full cell obtained from Medtronic Company for ARC testing compared to a 5 cent Canadian coin.

5.2.3 STUDIES OF THE REACTIVITY BETWEEN AGED CHARGED ELECTRODES AND ELECTROLYTES AT ELEVATED TEMPERATURES

The charged electrodes prepared using the protocol described in Chapter 2 can be regarded as fresh electrodes because the pellet cells were not cycled or stored for a relatively long time. However, aging of lithium ion cells is being more and more of a concern because most applications require a long life time. Broussely et al.[3] showed two types of aging situations for Li-ion cells: on storage and on cycling (during use). Aging during storage is caused by reactions between charged electrode materials and electrolyte while aging during cycling adds some kinetically induced factors such as volume variations of electrode materials which affect the integrity of passivation layers. The interphase between the electrolyte and electrode after cycling or storage may be different than that without cycling or storage because the interphase is the place where side reactions occur and most additives effect. Therefore, it is important to study the

reactivity between aged charged electrodes and electrolytes at elevated temperatures in future. Electrodes extracted from pouch cells can be used for this study.

REFERENCES

1. R. Van Noorden, *Nature*, **507**, 26–28 (2014).

2. D. L. Anderson, thesis, Duke University (2009).

3. M. Broussely, P. Biensan, F. Bonhomme, P. Blanchard, S. Herreyre, K. Nechev, and R. J. Staniewicz, *J. Power Sources*, **146**, 90–96 (2005).

4. S. S. Zhang, *J. Power Sources*, **162**, 1379–1394 (2006).

5. D. Xiong, J. C. Burns, A. J. Smith, N. Sinha, and J. R. Dahn, *J. Electrochem. Soc.*, **158**, A1431–A1435 (2011).

6. J. C. Burns, G. Jain, A. J. Smith, K. W. Eberman, E. Scott, J. P. Gardner, and J. R. Dahn, *J. Electrochem. Soc.*, **158**, A255–A261 (2011).

7. J. Xia, N. N. Sinha, L. P. Chen, G. Y. Kim, D. J. Xiong, and J. R. Dahn, *J. Electrochem. Soc.*, **161**, A84–A88 (2014).

8. J. Xia, N. N. Sinha, L. P. Chen, and J. R. Dahn, *J. Electrochem. Soc.*, **161**, A264–A274 (2014).

9. M. Xu, D. Lu, A. Garsuch, and B. L. Lucht, *J. Electrochem. Soc.*, **159**, A2130–A2134 (2012).

10. R. E. Peter and J. O. Christopher, *Electrochem. Soc. Interface*, **21**, 45 (2012).

11. M. N. Richard and J. R. Dahn, *J. Electrochem. Soc.*, **146**, 2068–2077 (1999).

12. M. N. Richard and J. R. Dahn, *J. Electrochem. Soc.*, **146**, 2078–2084 (1999).

13. D. D. MacNeil, D. Larcher, and J. R. Dahn, *J. Electrochem. Soc.*, **146**, 3596–3602 (1999).

14. F. Zhou, X. Zhao, and J. R. Dahn, *J. Electrochem. Soc.*, **156**, A343–A347 (2009).

15. X. Xia, P. Ping, and J. R. Dahn, *J. Electrochem. Soc.*, **159**, A1834–A1837 (2012).

16. J. S. Gnanaraj, E. Zinigrad, L. Asraf, H. E. Gottlieb, M. Sprecher, D. Aurbach, and M. Schmidt, *J. Power Sources*, **119–121**, 794–798 (2003).

17. T. Reddy, *Linden's Handbook of Batteries 4th Edition*, McGraw Hill Professional, (2010).

18. P. Arora and Z. (John) Zhang, *Chem. Rev.*, **104**, 4419–4462 (2004).

19. J. Choi and A. Manthiram, *Electrochem. Solid-State Lett.*, **8**, C102–C105 (2005).

20. A. J. Smith, J. C. Burns, and J. R. Dahn, *Electrochem. Solid-State Lett.*, **13**, A177–A179 (2010).

21. A. J. Smith, J. C. Burns, and J. R. Dahn, *Electrochem. Solid-State Lett.*, **14**, A39–A41 (2011).

22. E. Peled, *J. Electrochem. Soc.*, **126**, 2047–2051 (1979).

23. A. J. Smith, J. C. Burns, X. Zhao, D. Xiong, and J. R. Dahn, *J. Electrochem. Soc.*, **158**, A447–A452 (2011).

24. M. Armand and J.-M. Tarascon, *Nature*, **451**, 652–657 (2008).

25. O. K. Park, Y. Cho, S. Lee, H.-C. Yoo, H.-K. Song, and J. Cho, *Energy Environ. Sci.*, **4**, 1621–1633 (2011).

26. K. Ozawa, *Solid State Ion.*, **69**, 212–221 (1994).

27. A. Rougier, I. Saadoune, P. Gravereau, P. Willmann, and C. Delmasa, *Solid State Ion.*, **90**, 83–90 (1996).

28. Y. Wang, J. Jiang, and J. R. Dahn, *Electrochem. Commun.*, **9**, 2534–2540 (2007).

29. D. D. MacNeil, Z. Lu, and J. R. Dahn, *J. Electrochem. Soc.*, **149**, A1332–A1336 (2002).

30. J.-M. Kim and H.-T. Chung, *Electrochimica Acta*, **49**, 937–944 (2004).

31. T. Ohzuku and Y. Makimura, *Chem. Lett.*, **30**, 642–643 (2001).

32. R. A. Huggins, *Advanced Batteries Materials Science Aspects*, Springer Science, (2009).

33. T. Ohzuku, A. Ueda, and N. Yamamoto, *J. Electrochem. Soc.*, **142**, 1431–1435 (1995).

34. M. Winter and J. O. Besenhard, *Electrochimica Acta*, **45**, 31–50 (1999).

35. N. Tamura, R. Ohshita, M. Fujimoto, S. Fujitani, M. Kamino, and I. Yonezu, *J. Power Sources*, **107**, 48–55 (2002).

36. J. Li and J. R. Dahn, *J. Electrochem. Soc.*, **154**, A156–A161 (2007).

37. M. N. Obrovac and L. Christensen, *Electrochem. Solid-State Lett.*, **7**, A93–A96 (2004).

38. K. Xu, *Chem. Rev.*, **104**, 4303–4418 (2004).

39. M. Hu, X. Pang, and Z. Zhou, *J. Power Sources*, **237**, 229–242 (2013).

40. A. Abouimrane, I. Belharouak, and K. Amine, *Electrochem. Commun.*, **11**, 1073–1076 (2009).

41. H. Duncan, N. Salem, and Y. Abu-Lebdeh, *J. Electrochem. Soc.*, **160**, A838–A848 (2013).

42. S. S. Zhang and T. R. Jow, *J. Power Sources*, **109**, 458–464 (2002).

43. C. L. Campion, W. Li, and B. L. Lucht, *J. Electrochem. Soc.*, **152**, A2327–A2334 (2005).

44. A. B. McEwen, H. L. Ngo, K. LeCompte, and J. L. Goldman, *J. Electrochem. Soc.*, **146**, 1687–1695 (1999).

45. K. Xu, *J. Electrochem. Soc.*, **155**, A733–A738 (2008).

46. J. L. Nowinski, P. Lightfoot, and P. G. Bruce, *J. Mater. Chem.*, **4**, 1579–1580 (1994).

47. Y. Yamada, K. Furukawa, K. Sodeyama, K. Kikuchi, M. Yaegashi, Y. Tateyama, and A. Yamada, *J. Am. Chem. Soc.*, **136**, 5039–5046 (2014).

48. S. S. Zhang, *J. Power Sources*, **162**, 1379–1394 (2006).

49. H. Ota, Y. Sakata, A. Inoue, and S. Yamaguchi, *J. Electrochem. Soc.*, **151**, A1659–A1669 (2004).

50. Y. Hu, W. Kong, H. Li, X. Huang, and L. Chen, *Electrochem. Commun.*, **6**, 126–131 (2004).

51. I. A. Profatilova, S.-S. Kim, and N.-S. Choi, *Electrochimica Acta*, **54**, 4445–4450 (2009).

52. A. Sano and S. Maruyama, *J. Power Sources*, **192**, 714–718 (2009).

53. J. C. Burns, X. Xia, and J. R. Dahn, *J. Electrochem. Soc.*, **160**, A383–A386 (2013).

54. Z. Zhang, L. Hu, H. Wu, W. Weng, M. Koh, P. C. Redfern, L. A. Curtiss, and K. Amine, *Energy Environ. Sci.*, **6**, 1806–1810 (2013).

55. A. von Cresce and K. Xu, *J. Electrochem. Soc.*, **158**, A337–A342 (2011).

56. G. Yan, X. Li, Z. Wang, H. Guo, and C. Wang, *J. Power Sources*, **248**, 1306–1311 (2014).

57. S. R. Li, N. N. Sinha, C. H. Chen, K. Xu, and J. R. Dahn, *J. Electrochem. Soc.*, **160**, A2014–A2020 (2013).

58. A. M. Andersson and K. Edström, *J. Electrochem. Soc.*, **148**, A1100–A1109 (2001).

59. M. Nie, D. Chalasani, D. P. Abraham, Y. Chen, A. Bose, and B. L. Lucht, *J. Phys. Chem. C*, **117**, 1257–1267 (2013).

60. D. Aurbach, M. Koltypin, and H. Teller, *Langmuir*, **18**, 9000–9009 (2002).

61. M. Nie and B. L. Lucht, *J. Electrochem. Soc.*, **161**, A1001–A1006 (2014).

62. D. Aurbach, K. Gamolsky, B. Markovsky, Y. Gofer, M. Schmidt, and U. Heider, *Electrochimica Acta*, **47**, 1423–1439 (2002).

63. D. Aurbach, B. Markovsky, G. Salitra, E. Markevich, Y. Talyossef, M. Koltypin, L. Nazar, B. Ellis, and D. Kovacheva, *J. Power Sources*, **165**, 491–499 (2007).

64. L. Yang, B. Ravdel, and B. L. Lucht, *Electrochem. Solid-State Lett.*, **13**, A95–A97 (2010).

65. R. Dedryvère, D. Foix, S. Franger, S. Patoux, L. Daniel, and D. Gonbeau, *J. Phys. Chem. C*, **114**, 10999–11008 (2010).

66. T. Zheng, J. N. Reimers, and J. R. Dahn, *Phys. Rev. B*, **51**, 734–741 (1995).

67. A. Mabuchi, H. Fujimoto, K. Tokumitsu, and T. Kasuh, *J. Electrochem. Soc.*, **142**, 3049–3051 (1995).

68. D. D. MacNeil and J. R. Dahn, *J. Electrochem. Soc.*, **148**, A1205–A1210 (2001).

69. J. Jiang and J. R. Dahn, *Electrochimica Acta*, **49**, 4599–4604 (2004).

70. D. D. MacNeil, Ph.D Thesis, Dalhousie University (2001).

71. J. Jiang, Ph.D Thesis, Dalhousie University (2005).

72. C.H. Bamford and C.F.H. Tipper, Ed., in *Comprehensive Chemical Kinetics*, Reactions in the Solid State., vol. Volume 22, p. 41–113, Elsevier (1980)

73. D. I. Townsend and J. C. Tou, *Thermochim. Acta*, **37**, 1–30 (1980).

74. A. D. Little, *ARC-2000 TM Accelerating Rate Calorimeter-Operation, Maintenance and Parts Manual*, (1996).

75. J. C. Oxley, J. L. Smith, E. Rogers, W. Ye, A. A. Aradi, and T. J. Henly, *Energy Fuels*, **14**, 1252–1264 (2000).

76. E. Gimzewski and G. Audley, *Thermochim. Acta*, **214**, 129–140 (1993).

77. J. C. M. Torfs, L. Deij, A. J. Dorrepaal, and J. C. Heijens, *Anal. Chem.*, **56**, 2863–2867 (1984).

78. S. Brunauer, P. H. Emmett, and E. Teller, *J. Am. Chem. Soc.*, **60**, 309–319 (1938).

79. D. D. MacNeil, T. D. Hatchard, and J. R. Dahn, *J. Electrochem. Soc.*, **148**, A663–A667 (2001).

80. V. Etacheri, O. Haik, Y. Goffer, G. A. Roberts, I. C. Stefan, R. Fasching, and D. Aurbach, *Langmuir*, **28**, 965–976 (2012).

81. E. Markevich, G. Salitra, K. Fridman, R. Sharabi, G. Gershinsky, A. Garsuch, G. Semrau, M. A. Schmidt, and D. Aurbach, *Langmuir*, **30**, 7414–7424 (2014).

82. J. C. Burns, R. Petibon, K. J. Nelson, N. N. Sinha, A. Kassam, B. M. Way, and J. R. Dahn, *J. Electrochem. Soc.*, **160**, A1668–A1674 (2013).

83. C. P. Aiken, J. Xia, D. Y. Wang, D. A. Stevens, S. Trussler, and J. R. Dahn, *J. Electrochem. Soc.*, **161**, A1548–A1554 (2014).

84. Kathlyne Nelson, Master Thesis, Dalhousie University (2014).

85. J. Xia, L. Ma, C. P. Aiken, K. J. Nelson, L. P. Chen, and J. R. Dahn, *J. Electrochem. Soc.*, **161**, A1634–A1641 (2014).

86. J. Xia, D. Y. Wang, L. Ma, L. Downie, R. Petibon, K. Nelson, and J. Dahn, Electrolyte Additives for Li-ion cells, US Provisional Patent , 61974993, 2014.